Time Reversal Super Resolution in Randomly Layered Media

Jean-Pierre Fouque

Department of Statistics and Applied Probability, University of California, Santa Barbara, CA 93106-3110.

Josselin Garnier

Laboratoire de Probabilités et Modèles Aléatoires & Laboratoire Jacques-Louis Lions, Université Paris VII, 2 Place Jussieu, 75251 Paris Cedex 05, France.

Knut Sølna

Department of Mathematics, University of California, Irvine CA 92697

Abstract

In this paper we extend previous work on time reversal in randomly layered media [Fouque *et al*, Wave Motion **42**, 238-260 (2005)]. We consider first the case of an active source embedded below the surface in a finely layered random medium. We carry out time reversal with a time reversal mirror placed at the surface and we consider here the case where this mirror is larger than the carrier wavelength. In contrast with the situation addressed in our previous paper, where the size of the mirror was comparable to the wavelength, we show that multipathing dramatically enhances the effective aperture of the mirror so that super resolution at the location of the source can be obtained. In other words, the focal spot radius of the refocused field obtained in the case of a multiply scattering medium is much smaller than the spot size obtained in the case of a homogeneous medium. This super resolution effect is obtained by time-reversing the long incoherent waves generated by the multiple scattering due to the thin layers. We also give an application to the problem of focusing on a passive scatterer buried in the random medium and illuminated by a source at the surface.

Key words: Acoustic waves, random media, time reversal, super resolution.

Email addresses: fouque@pstat.ucsb.edu (Jean-Pierre Fouque), garnier@math.jussieu.fr (Josselin Garnier), ksolna@math.uci.edu (Knut Sølna).

1 Introduction

Time reversal super resolution effects for waves propagating in heterogeneous media have been observed and studied experimentally in various contexts, e.g. ultrasound and underwater acoustics. In [17] super-focusing for phase conjugation in random media is discussed for the first time. In [10] super-focusing with time reversal is experimentally observed. Super-focusing or super resolution is characterized by a focal spot that is narrower than the spot size predicted by the Rayleigh formula in homogeneous space [7]. It is important to understand this effect since time reversal has important potential applications in various fields, for instance imaging [22,13], communication [11], and destruction of tumors and kidney stones [12]. The mathematical understanding of time reversal in heterogeneous and highly-scattering media has been the topic of recent research. The one-dimensional situation where only time re-compression can occur due to geometry is well understood [9]. Time reversal in the three-dimensional case has been studied in different regimes of separation of scales: [2,4,19,5] in the parabolic regime, [3] in the radiative transfer regime, [15,14] in the randomly layered case. Indeed, three-dimensional randomly layered media are amongst the few models that can be quantitatively analyzed. It is a model where strong fluctuations can be addressed. It is a regime where backscattering and localization can be taken into account. It is the regime where time reversal in reflection can be studied. Finally, it is a model that is physically relevant for instance in the context of propagation through sedimentary layers. In [14] we studied the problem of the detection of a source using a small time reversal mirror of size comparable to the wavelength. In that case spatial refocusing takes place along rings due to the layered structure. The case of a large mirror is considered in [6] where an application to imaging in randomly layered media is given by using statistically stable coherent front waves. In this paper we also consider the case of a large mirror and we propose an application to the adaptive focusing on a strong scatterer buried in a randomly layered medium. We show that super resolution can be achieved on the scatterer by time reversing incoherent reflected waves and creating an aperture enhancement due to multi-pathing. We discuss the basic properties of time reversal in three dimensional randomly layered media and we compare the fundamental diffraction limit phenomenon in the homogeneous and random cases.

In the first part of the paper, an active source located inside the medium emits a pulse that is recorded on a time reversal mirror. The wave is sent back into the medium, either numerically in a computer with the knowledge of the medium, or physically into the real medium. The goal of this paper is to give a precise description of the refocusing of the pulse. In the regime of separation of scales that we consider, we show that the pulse refocuses at the original location of the source and at a critical time. In fact, time reversal refocusing contains information about the source which cannot be obtained

by a direct arrival time analysis. The resolution at the source can be enhanced by the randomness in the medium, this is sometimes referred to as a **super resolution** effect.

We consider the regime where the typical wavelength of the pulse emitted by the source is large relative to the correlation length of the medium, but short relative to the depth of the source. In this paper we first study wave propagation in a three dimensional layered medium in the case where the source is inside of the medium. We then consider time reversal of the wave emanating from the source and we analyze the refocusing properties of the wave field. We consider acoustic waves propagating in three spatial dimensions using the linearized equations of momentum and mass conservation:

$$\rho \frac{\partial \vec{\mathbf{u}}}{\partial t} + \nabla p = \vec{\mathbf{F}}, \qquad \frac{1}{K}\frac{\partial p}{\partial t} + \nabla . \vec{\mathbf{u}} = 0, \tag{1}$$

where p is the pressure, $\vec{\mathbf{u}}$ is the velocity, ρ is the density of the medium and K is the bulk modulus. The forcing term $\vec{\mathbf{F}}$ is due to the source. We consider the case with a constant density (for simplicity) and a randomly fluctuating bulk modulus in the slab $-L \leq z \leq 0$. Furthermore we assume that these fluctuations are only z-dependent, so that the medium is layered in that direction. Note that by hyperbolicity of the system of governing equations we can choose L large enough so that the termination of the slab does not affect the wave field at the surface $z = 0$ over the finite time period that we consider. We therefore consider the model

$$\rho \equiv \bar{\rho}, \qquad \frac{1}{K} = \begin{cases} \dfrac{1}{\bar{K}}\left(1 + \nu\left(\dfrac{z}{\varepsilon^2}\right)\right) & \text{if } z \in [-L, 0], \\ \dfrac{1}{\bar{K}} & \text{if } z \in (-\infty, -L) \cup (0, \infty), \end{cases} \tag{2}$$

where ν is a zero-mean mixing process and ε^2 is a small dimensionless parameter that characterizes the ratio between the correlation length of the medium and the typical depth of the source. A source located at $(\mathbf{x}_s, z_s)$, $z_s \leq 0$, generates a short pulse at time t_s. This is modeled by the forcing term $\vec{\mathbf{F}}$ given by:

$$\vec{\mathbf{F}}(t, \mathbf{x}, z) = \varepsilon^2 \vec{\mathbf{f}}\left(\frac{t - t_s}{\varepsilon}, \mathbf{x} - \mathbf{x}_s\right) \delta(z - z_s), \tag{3}$$

where we distinguish the transverse spatial coordinates $\mathbf{x} = (x, y)$ and the longitudinal coordinate z. In this modeling, the reference length is the depth $|z_s|$ and the reference time is the travel time $|z_s|/\bar{c}$, where $\bar{c} = \sqrt{\bar{K}/\bar{\rho}}$. These two reference scales are of order one. Compared to the reference time, the time duration of the source is short and proportional to ε. Compared to the

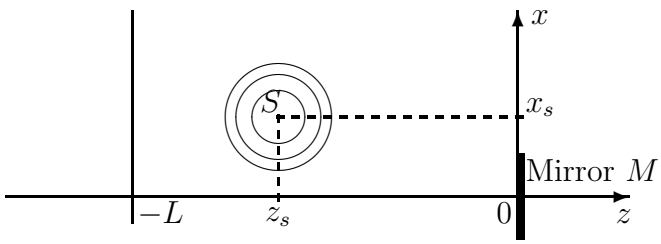

Fig. 1. Geometry of the experiment and emission from a point source.

reference length, the correlation length of the medium is very small and proportional to ε^2. Note that 1) The typical wavelength of the source is of order ε, which is large compared to the correlation length but small compared to the propagation distance. 2) the amplitude factor ε^2 has been added in (3) so that our quantities of interest will be of order one, but it plays no fundamental role as the wave equations are linear.

In our time reversal setup we place a time reversal mirror of spatial size $\mathcal{O}(1)$ at the origin. Our setup is illustrated by the cartoon given in Figure 1. In Section 2 we give the integral representation for the field generated by a source. The integral representation is obtained by taking a Fourier transform in the time and lateral space coordinates. In Section 3 we present the time reversal setup and we compute the integral representation of the time reversed field. In Section 4 we consider the case of a homogeneous medium and we compute in particular the size of the refocused spot size. In Section 5 we analyze time reversal with a source embedded in a randomly layered medium with a mirror at the surface. We carry out a careful stationary phase analysis combined with classic diffusion approximation results in the limit of small ε. This gives a limit for the time reversed wave field which reveals a refocusing of the pulse at a critical time and at the original source location. In order to illustrate the so-called super resolution effect, we compute the focal spot size for some specific random medium configurations and compare with the results obtained in the homogeneous medium case. The theoretical formulas are based on a description of the moments of the mode dependent reflection and transmission coefficients presented in [14]. We finally extend these results to the case of an embedded scatterer illuminated by a source located at the surface in Section 6.

2 Wavefield generated by a point source

2.1 The Fourier representation

In the scaling that we consider, the typical wavelength of the source is small $\mathcal{O}(\varepsilon)$ and we use the following specific Fourier transform and its inverse with

respect to time and the transverse direction:

$$\hat{p}(\omega,\boldsymbol{\kappa},z)=\int\int p(t,\mathbf{x},z)e^{\frac{i\omega}{\varepsilon}(t-\boldsymbol{\kappa}.\mathbf{x})}dtd\mathbf{x}\,,$$
$$p(t,\mathbf{x},z)=\frac{1}{(2\pi\varepsilon)^3}\int\int\hat{p}(\omega,\boldsymbol{\kappa},z)e^{-\frac{i\omega}{\varepsilon}(t-\boldsymbol{\kappa}.\mathbf{x})}\omega^2 d\omega d\boldsymbol{\kappa}\,.$$

We denote by $\hat{\vec{\mathbf{f}}}$ the ordinary unscaled Fourier transform of the source profile:

$$\hat{\vec{\mathbf{f}}}(\omega,\boldsymbol{\kappa})=\int\vec{\mathbf{f}}(t,\mathbf{x})e^{i\omega(t-\boldsymbol{\kappa}.\mathbf{x})}dtd\mathbf{x},\quad \vec{\mathbf{f}}(t,\mathbf{x})=\frac{1}{(2\pi)^3}\int\hat{\vec{\mathbf{f}}}(\omega,\boldsymbol{\kappa})e^{-i\omega(t-\boldsymbol{\kappa}.\mathbf{x})}\omega^2 d\omega d\boldsymbol{\kappa}.$$

The effective sound speed is $\bar{c}=\sqrt{\bar{K}/\bar{\rho}}$ and, with the notation $\kappa=|\boldsymbol{\kappa}|$, the effective mode-dependent longitudinal velocity $\bar{c}(\kappa)$ and the mode-dependent acoustic impedance $\bar{I}(\kappa)$ are given by

$$\bar{c}(\kappa)=\frac{\bar{c}}{\sqrt{1-\bar{c}^2\kappa^2}},\qquad \bar{I}(\kappa)=\bar{\rho}\bar{c}(\kappa). \tag{4}$$

We shall address different configurations in this paper, including active sources and passive scatterers. We shall see that, by using appropriate integral representations, it is possible to reduce the problem to the computations of 1) the field generated at the surface by a source located in the medium and/or 2) the field generated in the medium by a source located at the surface. In the next two sections, we give the general formulas for these two situations.

2.2 Field generated at the surface by an internal point source

In this subsection we consider the source (3) located inside the medium (meaning $z_s<0$). We focus our attention to the wave at the surface $z=0$ denoted by $(\vec{\mathbf{u}}_s,p_s)$. The integral representation of the field has been obtained in [14] (Equation (21)):

$$p_s(t,\mathbf{x})=\frac{1}{(2\pi\varepsilon)^3}\int\frac{\sqrt{\bar{I}(\kappa)}}{2}a(\omega,\boldsymbol{\kappa},0)e^{-\frac{i\omega}{\varepsilon}(t-\boldsymbol{\kappa}.\mathbf{x})}\omega^2 d\omega d\boldsymbol{\kappa}, \tag{5}$$
$$u_s(t,\mathbf{x})=\frac{1}{(2\pi\varepsilon)^3}\int\frac{1}{2\sqrt{\bar{I}(\kappa)}}a(\omega,\boldsymbol{\kappa},0)e^{-\frac{i\omega}{\varepsilon}(t-\boldsymbol{\kappa}.\mathbf{x})}\omega^2 d\omega d\boldsymbol{\kappa}, \tag{6}$$
$$\mathbf{v}_s(t,\mathbf{x})=\frac{1}{(2\pi\varepsilon)^3}\int\frac{\sqrt{\bar{I}(\kappa)}}{2\bar{\rho}}\boldsymbol{\kappa}a(\omega,\boldsymbol{\kappa},0)e^{-\frac{i\omega}{\varepsilon}(t-\boldsymbol{\kappa}.\mathbf{x})}\omega^2 d\omega d\boldsymbol{\kappa}, \tag{7}$$

where $\vec{\mathbf{u}}_s=(\mathbf{v}_s,u_s)$, and

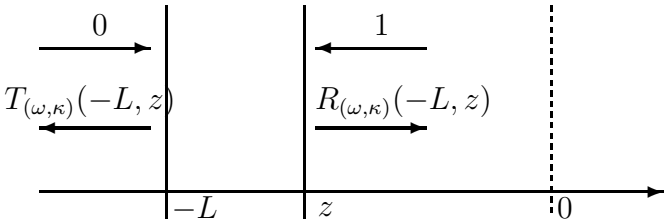

Fig. 2. Reflection and transmission coefficients.

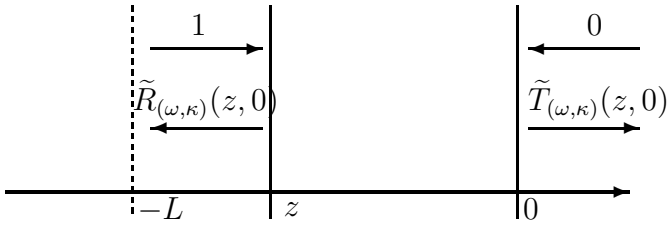

Fig. 3. Adjoint reflection and transmission coefficients.

$$a(\omega,\boldsymbol{\kappa},0)=\varepsilon^3 e^{\frac{i\omega}{\varepsilon}(t_s-\boldsymbol{\kappa}.\mathbf{x}_s)}\left[e^{-\frac{i\omega z_s}{\varepsilon\bar{c}(\kappa)}}T_g(\omega,\kappa,z_s)S_a(\omega,\boldsymbol{\kappa})\right.$$
$$\left.-e^{\frac{i\omega z_s}{\varepsilon\bar{c}(\kappa)}}R_g(\omega,\kappa,z_s)S_b(\omega,\boldsymbol{\kappa})\right]. \tag{8}$$

The source contributions are given by

$$S_a(\omega,\boldsymbol{\kappa})=\frac{\sqrt{\bar{I}(\kappa)}}{\bar{\rho}}\boldsymbol{\kappa}.\hat{\mathbf{f}}_{\mathbf{x}}(\omega,\boldsymbol{\kappa})+\frac{1}{\sqrt{\bar{I}(\kappa)}}\hat{f}_z(\omega,\boldsymbol{\kappa}), \tag{9}$$

$$S_b(\omega,\boldsymbol{\kappa})=\frac{\sqrt{\bar{I}(\kappa)}}{\bar{\rho}}\boldsymbol{\kappa}.\hat{\mathbf{f}}_{\mathbf{x}}(\omega,\boldsymbol{\kappa})-\frac{1}{\sqrt{\bar{I}(\kappa)}}\hat{f}_z(\omega,\boldsymbol{\kappa}), \tag{10}$$

where we have introduced the transverse and longitudinal source components defined by $\vec{\mathbf{f}}=(\mathbf{f}_{\mathbf{x}},f_z)$. The coefficients R_g and T_g are generalized versions of the standard reflection and transmission coefficients used in classical papers [1]. The coefficients $T_{(\omega,\kappa)}(-L,z)$ and $R_{(\omega,\kappa)}(-L,z)$ for a slab $[-L,z]$ are the usual transmission and reflection coefficients for the experiment corresponding to a left-going input wave incoming from the right (see Figure 2). We also introduce $\widetilde{R}_{(\omega,\kappa)}$ and $\widetilde{T}_{(\omega,\kappa)}$ defined as the adjoint reflection and transmission coefficients for the experiment corresponding to a right-going input wave incoming from the left (see Figure 3). We can express the generalized coefficients R_g and T_g in terms of the usual reflection and transmission coefficients $R_{(\omega,\kappa)}$ and $T_{(\omega,\kappa)}$ and the adjoint coefficients $\tilde{R}_{(\omega,\kappa)}$ and $\tilde{T}_{(\omega,\kappa)}$:

$$R_g(\omega,\kappa,z)=\frac{\widetilde{T}_{(\omega,\kappa)}(z,0)R_{(\omega,\kappa)}(-L,z)}{1-\widetilde{R}_{(\omega,\kappa)}(z,0)R_{(\omega,\kappa)}(-L,z)}, \tag{11}$$

$$T_g(\omega,\kappa,z)=\frac{\widetilde{T}_{(\omega,\kappa)}(z,0)}{1-\widetilde{R}_{(\omega,\kappa)}(z,0)R_{(\omega,\kappa)}(-L,z)}. \tag{12}$$

The asymptotic analysis of the moments of these coefficients is presented in [14]. To sum-up the analysis carried out in [14], we can say that the transmitted signal comprise a coherent front wave of duration $\mathcal{O}(\varepsilon)$ corresponding to the duration of the source, and a long noisy coda part that is caused by the multiple scattering by the layers. These coda waves are part of, and play a crucial role in, the time reversal procedure that we describe next.

2.3 Field generated in the medium by a surface point source

We next discuss the case of a source of the form (3) located at the surface $z_s = 0$ and we also take $\mathbf{x}_s = \mathbf{0}$: $\vec{\mathbf{F}}(t,\mathbf{x},z) = \varepsilon^2\vec{\mathbf{g}}((t-t_s)/\varepsilon,\mathbf{x})\delta(z)$. Proceeding as in [14], we write the integral representation of the field inside the medium:

$$\begin{aligned} u(t,\mathbf{x},z)=\frac{-1}{(2\pi\varepsilon)^3}\int\frac{1}{2\sqrt{\bar{I}(\kappa)}}\tilde{S}_b(\omega,\boldsymbol{\kappa})\Big[R_g(\omega,\kappa,z)e^{\frac{i\omega z}{\varepsilon\bar{c}(\kappa)}} \\ +T_g(\omega,\kappa,z)e^{-\frac{i\omega z}{\varepsilon\bar{c}(\kappa)}}\Big]e^{-\frac{i\omega}{\varepsilon}(t-\boldsymbol{\kappa}.\mathbf{x})}\omega^2 d\omega d\boldsymbol{\kappa}. \end{aligned} \tag{13}$$

where the source term $\tilde{S}_b$ is defined as in (10):

$$\tilde{S}_b(\omega,\boldsymbol{\kappa})=\frac{\sqrt{\bar{I}(\kappa)}}{\bar{\rho}}\boldsymbol{\kappa}.\hat{\mathbf{g}}_{\mathbf{x}}(\omega,\boldsymbol{\kappa})-\frac{1}{\sqrt{\bar{I}(\kappa)}}\hat{g}_z(\omega,\boldsymbol{\kappa}).$$

The pressure and transverse velocity fields have similar integral representations, but we do not write them as they are not required in the forthcoming analysis.

3 Time reversal with an active point source

We consider the situation where a point source located inside the medium at $(\mathbf{x}_s, z_s)$, $z_s < 0$, emits a short pulse. The forcing term imposed by this source is of the form

$$\vec{\mathbf{F}}(t,\mathbf{x},z)=\varepsilon^2\vec{\mathbf{f}}\left(\frac{t-t_s}{\varepsilon}\right)\delta(\mathbf{x}-\mathbf{x}_s)\delta(z-z_s) \tag{14}$$

and it generates a wave at the surface as described in Subsection 2.2. The first step of the time reversal procedure consists in recording the velocity signal at

the surface $z = 0$ on the mirror $M = \{(\mathbf{x}, z), \mathbf{x} \in D, z = 0\}$ during some time interval centered at $t = 0$. The shape of the mirror whose center is located at the point $\mathbf{0}$ is given by $D \subset \mathbb{R}^2$, which is a domain with a diameter of order one. It turns out that, as $\varepsilon \to 0$, the interesting asymptotic regime arises when we record the signal during a large time interval whose duration is of order one and is denoted by t_1 with $t_1 > 0$. Note that, in a source detection problem, t_s, $\mathbf{x}_s$, and z_s are unknown quantities.

In the second step of the time reversal procedure, a piece of the recorded signal is clipped using a cut-off function $s \mapsto G_1(s)$ where the support of G_1 is included in $[-t_1/2, t_1/2]$. We denote the recorded part of the wave by $\vec{\mathbf{u}}_{rec}$ so that

$$\vec{\mathbf{u}}_{rec}(t, \mathbf{x}) = \vec{\mathbf{u}}_s(t, \mathbf{x}) G_1(t) G_2(\mathbf{x}), \tag{15}$$

where G_2 is the spatial cut-off function introduced by the mirror $G_2(\mathbf{x}) = \mathbf{1}_D(\mathbf{x})$, and D is the shape of the mirror. We then time reverse this piece of signal and send it back into the same medium. This means that we consider a new problem defined by the acoustic equations (1) with the source term

$$\vec{\mathbf{F}}_{TR}(t, \mathbf{x}, z) = \vec{\mathbf{f}}_{TR}(t, \mathbf{x}) \delta(z), \quad \vec{\mathbf{f}}_{TR}(t, \mathbf{x}) = \bar{\rho}\bar{c} \vec{\mathbf{u}}_{rec}(-t, \mathbf{x}), \tag{16}$$

where TR stands for "Time Reversal" and the factor $\bar{\rho}\bar{c}$ has been added to restore the physical dimension of the expression. Note that by linearity of the problem this factor plays no role in the analysis.

By using successively (16), (15), (7) and (6), we obtain

$$\hat{\mathbf{f}}_{TR,\mathbf{x}}(\omega, \boldsymbol{\kappa}) = \frac{\bar{\rho}\bar{c}}{(2\pi\varepsilon)^3} \int \frac{\sqrt{\bar{I}(\kappa')}}{2\bar{\rho}} \boldsymbol{\kappa}' \overline{a(\omega', \boldsymbol{\kappa}', 0)} \overline{\hat{G}_1\left(\frac{\omega - \omega'}{\varepsilon}\right)} \hat{G}_2\left(\frac{\omega \boldsymbol{\kappa} + \omega' \boldsymbol{\kappa}'}{\varepsilon}\right) \omega'^2 d\omega' d\boldsymbol{\kappa}',$$

$$\hat{f}_{TR,z}(\omega, \boldsymbol{\kappa}) = \frac{\bar{\rho}\bar{c}}{(2\pi\varepsilon)^3} \int \frac{1}{2\sqrt{\bar{I}(\kappa')}} \overline{a(\omega', \boldsymbol{\kappa}', 0)} \overline{\hat{G}_1\left(\frac{\omega - \omega'}{\varepsilon}\right)} \hat{G}_2\left(\frac{\omega \boldsymbol{\kappa} + \omega' \boldsymbol{\kappa}'}{\varepsilon}\right) \omega'^2 d\omega' d\boldsymbol{\kappa}',$$

where $a(\omega, \boldsymbol{\kappa}, 0)$ is given by (8), and the Fourier transforms of the window functions are defined by

$$\hat{G}_1(\omega) = \int G_1(t) e^{i\omega t} dt, \qquad \hat{G}_2(\mathbf{k}) = \int G_2(\mathbf{x}) e^{-i\mathbf{k}.\mathbf{x}} d\mathbf{x}.$$

The new incoming signal propagates into the same medium and produces the time reversed wave field. Here we derive an exact integral representation for this wave field which will be exploited in the following sections to analyze its refocusing properties.

Substituting the expressions for $\hat{\mathbf{f}}_{TR,\mathbf{x}}$ and $\hat{f}_{TR,z}$ into (13), we obtain the following representation of the longitudinal velocity

$$u_{TR}(t,\mathbf{x},z) = \frac{1}{(2\pi)^6\varepsilon^3}\int\int \frac{H_0(\boldsymbol{\kappa}_1,\boldsymbol{\kappa}_2)}{4\sqrt{\bar{I}(\kappa_1)}}\overline{\hat{G}_1\left(\frac{\omega_1-\omega_2}{\varepsilon}\right)}\hat{G}_2\left(\frac{\omega_1\boldsymbol{\kappa}_1+\omega_2\boldsymbol{\kappa}_2}{\varepsilon}\right)$$
$$\times e^{i\left(\frac{-(\omega_2 t_s+\omega_1 t)+(\omega_2\boldsymbol{\kappa}_2.\mathbf{x}_s+\omega_1\boldsymbol{\kappa}_1.\mathbf{x})}{\varepsilon}\right)}\left[\sum_{j=1}^{4}P_j\right]\omega_1^2\omega_2^2 d\omega_1 d\boldsymbol{\kappa}_1 d\omega_2 d\boldsymbol{\kappa}_2, \tag{17}$$

where we define the P_j's by

$$P_1 = -e^{i\left(-\frac{\omega_2 z_s}{\varepsilon\bar{c}(\kappa_2)}+\frac{\omega_1 z}{\varepsilon\bar{c}(\kappa_1)}\right)}\overline{R_g(\omega_2,\kappa_2,z_s)}R_g(\omega_1,\kappa_1,z)\overline{S_b(\omega_2,\boldsymbol{\kappa}_2)},$$
$$P_2 = e^{i\left(\frac{\omega_2 z_s}{\varepsilon\bar{c}(\kappa_2)}+\frac{\omega_1 z}{\varepsilon\bar{c}(\kappa_1)}\right)}\overline{T_g(\omega_2,\kappa_2,z_s)}R_g(\omega_1,\kappa_1,z)\overline{S_a(\omega_2,\boldsymbol{\kappa}_2)},$$
$$P_3 = e^{i\left(\frac{\omega_2 z_s}{\varepsilon\bar{c}(\kappa_2)}-\frac{\omega_1 z}{\varepsilon\bar{c}(\kappa_1)}\right)}\overline{T_g(\omega_2,\kappa_2,z_s)}T_g(\omega_1,\kappa_1,z)\overline{S_a(\omega_2,\boldsymbol{\kappa}_2)},$$
$$P_4 = -e^{i\left(-\frac{\omega_2 z_s}{\varepsilon\bar{c}(\kappa_2)}-\frac{\omega_1 z}{\varepsilon\bar{c}(\kappa_1)}\right)}\overline{R_g(\omega_2,\kappa_2,z_s)}T_g(\omega_1,\kappa_1,z)\overline{S_b(\omega_2,\boldsymbol{\kappa}_2)},$$

and where the function H_0 is given by

$$H_0(\boldsymbol{\kappa},\boldsymbol{\kappa}') = \frac{\bar{\rho}\bar{c}}{\sqrt{\bar{I}(\kappa)\bar{I}(\kappa')}} - \frac{\bar{c}\sqrt{\bar{I}(\kappa)\bar{I}(\kappa')}}{\bar{\rho}}\boldsymbol{\kappa}.\boldsymbol{\kappa}'. \tag{18}$$

Motivated by the presence of the terms $\hat{G}_1(\frac{\omega_1-\omega_2}{\varepsilon})$ and $\hat{G}_2\left(\frac{\omega_1\boldsymbol{\kappa}_1+\omega_2\boldsymbol{\kappa}_2}{\varepsilon}\right)$ we carry out the change of variables $\omega_1 = \omega+\varepsilon h/2$, $\omega_2 = \omega-\varepsilon h/2$, $\boldsymbol{\kappa}_1 = \boldsymbol{\kappa}+\varepsilon\boldsymbol{\lambda}/2$, $\boldsymbol{\kappa}_2 = -\boldsymbol{\kappa}+\varepsilon\boldsymbol{\lambda}/2$, which, to leading order, gives

$$u_{TR}(t,\mathbf{x},z) = \frac{1}{(2\pi)^6}\int\int \frac{H_0(\boldsymbol{\kappa},-\boldsymbol{\kappa})}{4\sqrt{\bar{I}(\kappa)}}\overline{\hat{G}_1(h)}\hat{G}_2\left(h\boldsymbol{\kappa}+\omega\boldsymbol{\lambda}\right)\left[\sum_{j=1}^{4}\tilde{P}_j\right]$$
$$\times e^{\frac{i\omega}{\varepsilon}(-(t_s+t)+\boldsymbol{\kappa}.(\mathbf{x}-\mathbf{x}_s))}e^{\frac{ih}{2}(t_s-t+\boldsymbol{\kappa}.(\mathbf{x}+\mathbf{x}_s))+\frac{i\omega}{2}\boldsymbol{\lambda}.(\mathbf{x}+\mathbf{x}_s)}\omega^4 d\omega dh d\boldsymbol{\kappa} d\boldsymbol{\lambda}, \tag{19}$$

with the $\tilde{P}_j$'s defined by

$$\tilde{P}_1 = -e^{\frac{-i\omega}{\varepsilon}\frac{z_s-z}{\bar{c}(\kappa)}}e^{\frac{ih}{2}\frac{z_s+z}{\bar{c}(\kappa)}-\frac{i\omega}{2}\boldsymbol{\lambda}.\boldsymbol{\kappa}\bar{c}(\kappa)(z_s+z)}\overline{R_g}R_g\,\overline{S_b(\omega,-\boldsymbol{\kappa})},$$
$$\tilde{P}_2 = e^{\frac{i\omega}{\varepsilon}\frac{z_s+z}{\bar{c}(\kappa)}}e^{-\frac{ih}{2}\frac{z_s-z}{\bar{c}(\kappa)}+\frac{i\omega}{2}\boldsymbol{\lambda}.\boldsymbol{\kappa}\bar{c}(\kappa)(z_s-z)}\overline{T_g}R_g\,\overline{S_a(\omega,-\boldsymbol{\kappa})},$$
$$\tilde{P}_3 = e^{\frac{i\omega}{\varepsilon}\frac{z_s-z}{\bar{c}(\kappa)}}e^{-\frac{ih}{2}\frac{z_s+z}{\bar{c}(\kappa)}+\frac{i\omega}{2}\boldsymbol{\lambda}.\boldsymbol{\kappa}\bar{c}(\kappa)(z_s+z)}\overline{T_g}T_g\,\overline{S_a(\omega,-\boldsymbol{\kappa})},$$
$$\tilde{P}_4 = -e^{-\frac{i\omega}{\varepsilon}\frac{z_s+z}{\bar{c}(\kappa)}}e^{\frac{ih}{2}\frac{z_s-z}{\bar{c}(\kappa)}-\frac{i\omega}{2}\boldsymbol{\lambda}.\boldsymbol{\kappa}\bar{c}(\kappa)(z_s-z)}\overline{R_g}T_g\,\overline{S_b(\omega,-\boldsymbol{\kappa})},$$

where the generalized reflection and transmission coefficients with the complex conjugate are evaluated at $(\omega - \varepsilon h/2, -\boldsymbol{\kappa} + \varepsilon\boldsymbol{\lambda}/2, z_s)$, and the other ones are evaluated at $(\omega + \varepsilon h/2, \boldsymbol{\kappa} + \varepsilon\boldsymbol{\lambda}/2, z)$, and where we have used that $\nabla_{\boldsymbol{\kappa}}\bar{c}(\kappa) = \bar{c}^3(\kappa)\boldsymbol{\kappa}$ from the definition (4). Note that, using the definition (18), we have $H_0(\boldsymbol{\kappa}, -\boldsymbol{\kappa}) = \bar{c}(\kappa)/\bar{c}$. In the following sections we study the asymptotic behavior of the time reversed wave field u_{TR}, the longitudinal velocity, in the limit $\varepsilon \to 0$.

4 Time reversal in homogeneous medium

We first examine the deterministic case with $\nu \equiv 0$ which corresponds to a source embedded in a homogeneous medium at the depth $z_s < 0$. The time reversed wave field is described by (19) with $R_g = 0$ and $T_g = 1$. In this case only the $\tilde{P}_3$ term contributes to u_{TR} which reduces to

$$u_{TR}(t,\mathbf{x},z) = \frac{1}{(2\pi)^6}\int\int \frac{\bar{c}(\kappa)}{4\bar{c}\sqrt{\bar{I}(\kappa)}}\overline{S_a(\omega,-\boldsymbol{\kappa})}\overline{\hat{G}_1(h)}\hat{G}_2\left(h\boldsymbol{\kappa}+\omega\boldsymbol{\lambda}\right) \tag{20}$$
$$\times e^{\frac{i\phi}{\varepsilon}} e^{\frac{ih}{2}\left(t_s-t+\boldsymbol{\kappa}.(\mathbf{x}+\mathbf{x}_s)-\frac{z_s+z}{\bar{c}(\kappa)}\right)+\frac{i\omega}{2}\left(\boldsymbol{\lambda}.(\mathbf{x}+\mathbf{x}_s)+\boldsymbol{\lambda}.\boldsymbol{\kappa}\bar{c}(\kappa)(z_s+z)\right)}\omega^4 d\omega dh d\boldsymbol{\kappa} d\boldsymbol{\lambda},$$

where the rapid phase is $\phi = \omega\left(-(t_s+t) + \boldsymbol{\kappa}.(\mathbf{x}-\mathbf{x}_s) + (z_s - z)/\bar{c}(\kappa)\right)$. Here the hypotheses that the mirror has a size of order one and that the recording time window is of order one become important. They show that the functions $\hat{G}_1$ and $\hat{G}_2$ do not have fast variations. We now apply the stationary phase method. There are three cases depending on the observation time t and the observation point $M = (\mathbf{x}, z)$. The first case corresponds to observing the wave front before it refocuses at the original source point, whereas the second case corresponds to an observation point on the wave front after it has refocused, and we show below that these two contributions are small of order ε. The third case corresponds to observing the wave front at the original source point and at the critical time, and the refocused wave is of order one.

• If $t < -t_s$, then there exists one stationary map given by $\boldsymbol{\kappa} = \boldsymbol{\kappa}_s$ and any ω, with

$$\boldsymbol{\kappa}_s = -\frac{1}{\bar{c}}\frac{\mathbf{x}-\mathbf{x}_s}{\sqrt{|z-z_s|^2+|\mathbf{x}-\mathbf{x}_s|^2}} = -\frac{1}{\bar{c}}\frac{\mathbf{x}-\mathbf{x}_s}{SM}, \tag{21}$$

if and only if the observation point M satisfies $z > z_s$ and $SM = \bar{c}|t+t_s|$. The stationary phase method gives that the value of the integral in (20) is of order ε.

• If $t > -t_s$, then there exists one stationary map given by $\boldsymbol{\kappa} = -\boldsymbol{\kappa}_s$ and any ω, if and only if the observation point M satisfies $z < z_s$ and $SM = \bar{c}(t + t_s)$. Again the stationary phase method gives that the value of the integral in (20) is of order ε.

• If $t = -t_s$, the critical time, there exists one stationary map if and only if $\mathbf{x} = \mathbf{x}_s$ and $z = z_s$, and the map is globally stationary meaning that the value of the integral in (20) is of order one. We thus consider an observation time t close to $-t_s$ and an observation point close to $(\mathbf{x}_s, z_s)$. This is done using the following parameterization

$$t = -t_s + \varepsilon T, \qquad \mathbf{x} = \mathbf{x}_s + \varepsilon \mathbf{X}, \text{ and } z = z_s + \varepsilon Z. \tag{22}$$

The integral representation of the refocused velocity field becomes

$$\begin{aligned} u_{TR}(t, \mathbf{x}, z) = \frac{1}{(2\pi)^6} \int\int \frac{\bar{c}(\kappa)}{4\bar{c}\sqrt{\bar{I}(\kappa)}} \overline{S_a(\omega, -\boldsymbol{\kappa})} \overline{\hat{G}_1(h)} \hat{G}_2 \left(h\boldsymbol{\kappa} + \omega \boldsymbol{\lambda}\right) \\ \times e^{i\omega\left(-T + \boldsymbol{\kappa}.\mathbf{X} - \frac{Z}{\bar{c}(\kappa)}\right)} e^{ih\left(t_s + \boldsymbol{\kappa}.\mathbf{x}_s - \frac{z_s}{\bar{c}(\kappa)}\right) + i\omega\left(\boldsymbol{\lambda}.\mathbf{x}_s + \boldsymbol{\lambda}.\boldsymbol{\kappa}\bar{c}(\kappa) z_s\right)} \omega^4 d\omega dh d\boldsymbol{\kappa} d\boldsymbol{\lambda} \end{aligned} \tag{23}$$

Next we apply the change of variables $\boldsymbol{\lambda} \mapsto \mathbf{k} = \omega \boldsymbol{\lambda} + h\boldsymbol{\kappa}$ and we integrate with respect to $\mathbf{k}$ and h to obtain

$$\begin{aligned} u_{TR}(t, \mathbf{x}, z) = \frac{1}{(2\pi)^3} \int\int \frac{\bar{c}(\kappa)}{4\bar{c}\sqrt{\bar{I}(\kappa)}} G_1 \left(t_s - z_s \frac{\bar{c}(\kappa)}{\bar{c}^2}\right) G_2 \left(\mathbf{x}_s + \boldsymbol{\kappa}\bar{c}(\kappa) z_s\right) \\ \times \overline{S_a(\omega, -\boldsymbol{\kappa})} e^{i\omega\left(-T + \boldsymbol{\kappa}.\mathbf{X} - \frac{Z}{\bar{c}(\kappa)}\right)} \omega^2 d\omega d\boldsymbol{\kappa}. \end{aligned} \tag{24}$$

Qualitatively, the mirror emits a converging spherical wave whose amplitude is of order ε and whose support at time $t < -t_s$ lies in the upper part of the sphere with center S and radius $\bar{c}(t+t_s)$. At the critical time $-t_s$ the refocusing occurs at the original source location S. The refocused pulse has an amplitude of order one and it is given by (24). After the time $-t_s$ a diverging spherical wave is going downwards from the point S (see Figure 4). We can be more precise and give quantitative information on the **focal spot**.

In order to simplify the formula and clarify the roles of the different quantities in the refocusing we assume that the source is concentrated in frequency in a narrow band around a large carrier frequency ω_0, and is located relatively far from the mirror. We choose the (x, y)-axes so that the lateral position of the source is $\mathbf{x}_s = (x_s, 0)$. These assumptions translate into

$$\vec{\mathbf{f}}(t) = \vec{\mathbf{f}}_0 \left(\frac{t}{T_w}\right) e^{i\omega_0 t} + c.c. \tag{25}$$

with $\omega_0 T_w \gg 1$ and $|z_s| \gg \sqrt{a^2+b^2}$, where T_w is the initial pulse width, a is the typical dimension of the mirror in the x-direction, and b is the typical dimension of the mirror in the y-direction. The function $\vec{\mathbf{f}}_0$ is the normalized envelope of the pulse profile. The spatial cut-off function determining the mirror has the form

$$G_2(\mathbf{x}) = g_2\left(\frac{x}{a}, \frac{y}{b}\right) \tag{26}$$

where g_2 is the normalized cut-off function. Then, after the change of variable $\boldsymbol{\kappa} \mapsto \mathbf{y} = \mathbf{x}_s + \boldsymbol{\kappa}\bar{c}(\kappa) z_s$ in (24), and integration with respect to $\mathbf{y}$, we get

$$\begin{aligned} u_{TR}(t,\mathbf{x},z) = & \frac{a^2 z_s \omega_0^2}{16\pi^2 \bar{c}^3 \bar{\rho} OS^4} \vec{\mathbf{OS}}.\vec{\mathbf{f}}_0 \left(-\frac{T}{T_w} + \frac{(\mathbf{X},Z).\vec{\mathbf{OS}}}{\bar{c} OS T_w}\right) e^{i\omega_0\left(-T + \frac{(\mathbf{X},Z).\vec{\mathbf{OS}}}{\bar{c} OS}\right)} \\ & \times G_1\left(t_s + \frac{OS}{\bar{c}}\right) \hat{g}_2\left(\frac{\omega_0 a |z_s|}{\bar{c} OS^3}(x_s Z - z_s X), \frac{\omega_0 b}{\bar{c} OS} Y\right) + c.c \end{aligned} \tag{27}$$

where $\vec{\mathbf{OS}}$ is the vector from the origin to the source. Note that the longitudinal refocused velocity field is nonzero only if the signal originating from the source has been recorded by the mirror, meaning that $t_s + OS/\bar{c}$ lies in the support of G_1. The focal shape depends on the Fourier transform of the mirror shape and the initial pulse profile. We introduce the new orthonormal frame $(\vec{\mathbf{e}}_1, \vec{\mathbf{e}}_2, \vec{\mathbf{e}}_3)$ defined by

$$\vec{\mathbf{e}}_1 = \frac{1}{OS}\begin{pmatrix} -z_s \\ 0 \\ x_s \end{pmatrix}, \qquad \vec{\mathbf{e}}_2 = \begin{pmatrix} 0 \\ 1 \\ 0 \end{pmatrix}, \qquad \vec{\mathbf{e}}_3 = \frac{1}{OS}\begin{pmatrix} x_s \\ 0 \\ z_s \end{pmatrix},$$

and described in the left picture of Figure 9. The pulse shape shown in Figure 6 is, up to a multiplicative factor

$$|u_{TR}(t,\mathbf{x},z)| = \left|\frac{\vec{\mathbf{OS}}}{OS}.\vec{\mathbf{f}}_0\left(-\frac{T}{T_w} + \frac{(\mathbf{X},Z).\vec{\mathbf{e}}_3}{\bar{c} T_w}\right)\right| \left|\hat{g}_2\left(\frac{\omega_0 a |z_s|}{\bar{c} OS^2}(\mathbf{X},Z).\vec{\mathbf{e}}_1, \frac{\omega_0 b}{\bar{c} OS}(\mathbf{X},Z).\vec{\mathbf{e}}_2\right)\right|.$$

- In the $\vec{\mathbf{e}}_3$-direction (along the vector $\vec{\mathbf{OS}}$), the focal spot size is determined by the initial pulse width T_w and it is given by $R_3 = \bar{c} T_w$.

- In the two other directions, the focal spot size is determined by the mirror sizes a and b. In the $\vec{\mathbf{e}}_2$-direction, the focal spot has the size $R_2 = \lambda_0 OS/b$ where $\lambda_0 = 2\pi\bar{c}/\omega_0$ is the carrier wavelength of the pulse. In the $\vec{\mathbf{e}}_1$-direction, the focal spot has the size $R_1 = \lambda_0 OS^2/(a|z_s|)$. These formulas are consistent with the standard **Rayleigh resolution** formula, which claims that the focal spot of a beam with carrier wavelength λ_0 focused with a system of size a from

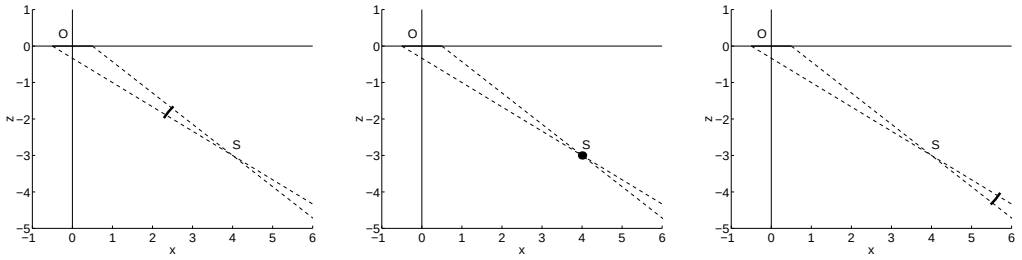

$t < -t_s$ $\qquad$ $t = -t_s$ $\qquad$ $t > -t_s$

Fig. 4. Pulse refocusing in homogeneous medium. The focal spot size depends on the numerical aperture which measures the angular diversity of the refocused waves which participate in the refocusing.

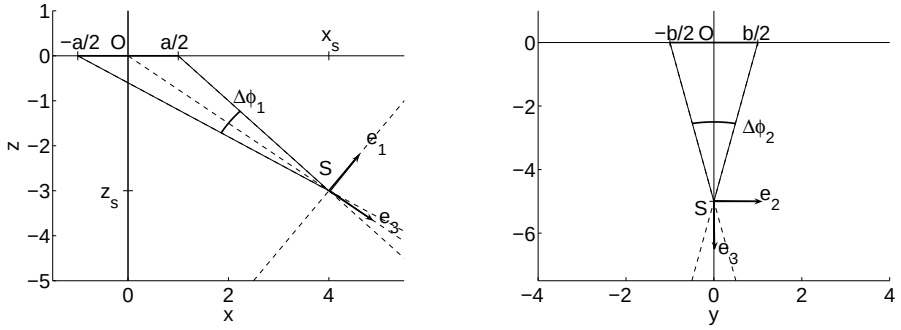

Fig. 5. Cones of aperture. The left plot shows the $(\vec{\mathbf{e}}_1, \vec{\mathbf{e}}_3)$-section of the cone of aperture. The right plot shows the $(\vec{\mathbf{e}}_2, \vec{\mathbf{e}}_3)$-section.

a distance L is of the order of $\lambda_0 L/a$ [7]. More precisely, we can rewrite the focal spot radii in terms of the numerical aperture of the waves that participate in the refocusing (see Figure 5). The spot sizes are given by $R_j = \lambda_0/\Delta\phi_j$, $j = 1, 2$, where

$$\Delta\phi_1 = \arctan\left(\frac{x_s + \frac{a}{2}}{|z_s|}\right) - \arctan\left(-\frac{x_s + \frac{a}{2}}{|z_s|}\right) \overset{|z_s|\gg a}{\simeq} \frac{|z_s|a}{OS^2}, \tag{28}$$

$$\Delta\phi_2 = \arctan\left(\frac{b}{2OS}\right) - \arctan\left(-\frac{b}{2OS}\right) \overset{|z_s|\gg a}{\simeq} \frac{b}{OS}. \tag{29}$$

5 Random Medium

Now we analyze the case with a random medium. We first consider the P_3 term in the expression (19) for the longitudinal velocity. As shown in [14] the generalized transmission coefficient depends only on the modulus of the slowness vector $\boldsymbol{\kappa}$, so we can write

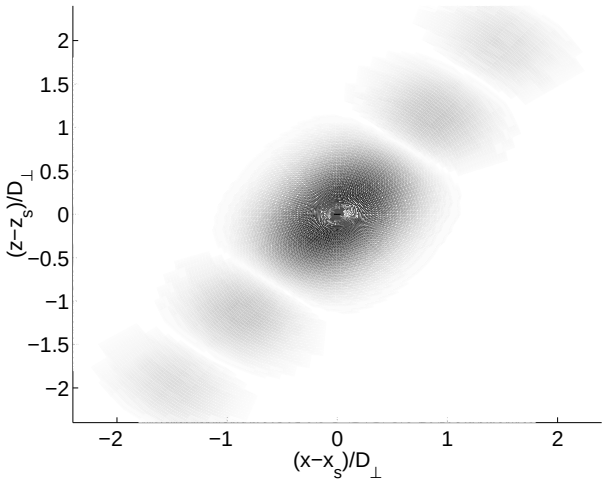

Fig. 6. Pulse shape in the plane $(\vec{\mathbf{e}}_1, \vec{\mathbf{e}}_3)$. The mirror is a rectangle with size a in the x-direction and size b in the y-direction, the initial source is vertical and emits a Gaussian pulse of duration T_w. As a result the spot shape is a sinc function with radius $D_\perp = \lambda_0/\Delta\phi_1$ with $\Delta\phi_1 = a|z_s|/OS^2$ in the $\vec{\mathbf{e}}_1$ direction and a Gaussian function with radius $\bar{c}T_w$ in the $\vec{\mathbf{e}}_3$ direction. It is also a sinc function with radius $\lambda_0/\Delta\phi_2$ with $\Delta\phi_2 = b/OS$ in the $\vec{\mathbf{e}}_2$ orthogonal direction (not shown here).

$$u_{TR}^{(3)}(t,\mathbf{x},z) = \frac{1}{(2\pi)^6}\int\int \frac{\bar{c}(\kappa)}{4\bar{c}\sqrt{\bar{I}(\kappa)}}\overline{S_a(\omega,-\boldsymbol{\kappa})}\overline{\hat{G}_1(h)}\hat{G}_2\left(h\boldsymbol{\kappa}+\omega\boldsymbol{\lambda}\right) \tag{30}$$
$$\times\overline{T_g\left(\omega-\varepsilon h/2,|-\boldsymbol{\kappa}+\varepsilon\boldsymbol{\lambda}/2|,z_s\right)}T_g\left(\omega+\varepsilon h/2,|\boldsymbol{\kappa}+\varepsilon\boldsymbol{\lambda}/2|,z\right)$$
$$\times e^{\frac{i\phi}{\varepsilon}}e^{\frac{ih}{2}\left(t_s-t+\boldsymbol{\kappa}.(\mathbf{x}+\mathbf{x}_s)-\frac{z_s+z}{\bar{c}(\kappa)}\right)+\frac{i\omega}{2}\left(\boldsymbol{\lambda}.(\mathbf{x}+\mathbf{x}_s)+\boldsymbol{\lambda}.\boldsymbol{\kappa}\bar{c}(\kappa)(z_s+z)\right)}\omega^4 d\omega dh d\boldsymbol{\kappa} d\boldsymbol{\lambda},$$

where the rapid phase is $\phi = \omega\left(-(t_s+t)+\boldsymbol{\kappa}.(\mathbf{x}-\mathbf{x}_s)+(z_s-z)/\bar{c}(\kappa)\right)$. As $\varepsilon\to 0$ the asymptotic behavior of this integral is governed by its fast phase and by the product of the two transmission coefficients which contains the effect of randomness. We first apply the stationary phase method and we will deal with the random part of the integral in a second step. The rapid phase is the same as in the homogeneous case and we find that the globally stationary point is determined by $t+t_s=0$, $\mathbf{x}=\mathbf{x}_s$, and $z=z_s$. We then consider an observation time t close to $-t_s$ and an observation point $(\mathbf{x},z)$ close to $(\mathbf{x}_s,z_s)$ according to the parameterization (22). The integral representation of the refocused velocity field is then

$$u_{TR}^{(3)}(t,\mathbf{x},z) = \frac{1}{(2\pi)^6}\int\int \frac{\bar{c}(\kappa)}{4\bar{c}\sqrt{\bar{I}(\kappa)}}\overline{S_a(\omega,-\boldsymbol{\kappa})}\overline{\hat{G}_1(h)}\hat{G}_2\left(h\boldsymbol{\kappa}+\omega\boldsymbol{\lambda}\right)$$
$$\times\overline{T_g\left(\omega-\varepsilon h/2,|-\boldsymbol{\kappa}+\varepsilon\boldsymbol{\lambda}/2|,z_s\right)}T_g\left(\omega+\varepsilon h/2,|\boldsymbol{\kappa}+\varepsilon\boldsymbol{\lambda}/2|,z_s+\varepsilon Z\right)$$
$$\times e^{i\omega\left(-T+\boldsymbol{\kappa}.\mathbf{X}-\frac{Z}{\bar{c}(\kappa)}\right)}e^{ih\left(t_s+\boldsymbol{\kappa}.\mathbf{x}_s-\frac{z_s}{\bar{c}(\kappa)}\right)+i\omega\left(\boldsymbol{\lambda}.\mathbf{x}_s+\boldsymbol{\lambda}.\boldsymbol{\kappa}\bar{c}(\kappa)z_s\right)}\omega^4 d\omega dh d\boldsymbol{\kappa} d\boldsymbol{\lambda}. \tag{31}$$

The effect of the randomness is contained in the product of the generalized transmission coefficients. In the next section we use the asymptotic analysis of

the autocorrelation function studied in [14] to deduce the refocusing properties of the pulse.

5.1 Expectation of the refocused pulse

The expectation of $u_{TR}^{(3)}(t,\mathbf{x},z)$ given in (31) involves the first moment of the product of generalized transmission coefficients. In [14] it is shown that the generalized transmission coefficients at two frequencies and slowness vectors are correlated only if the frequencies and the moduli of the slowness vectors are close to each other at order ε. More precisely, it is shown in [14] that, for any l and any h, we have

$$\begin{aligned}\mathbb{E}\left[\overline{T_g\left(\omega-\varepsilon h/2,\kappa-\varepsilon l/2,z_s\right)}T_g\left(\omega+\varepsilon h/2,\kappa+\varepsilon l/2,z_s+\varepsilon Z\right)\right] \\ \xrightarrow{\varepsilon\to 0}\int e^{i[h-\omega l\bar{c}(\kappa)^2\kappa]\tau}\mathcal{W}_g^{(-)}\left(\omega,\kappa,\tau\right)d\tau\end{aligned} \tag{32}$$

where

$$\mathcal{W}_g^{(-)}(\omega,\kappa,\tau)=\sum_{n=0}^{\infty}\left[\mathcal{W}_n(\cdot,\omega,\kappa,-L,z_s)*\mathcal{W}_n^{(T)}(\cdot,\omega,\kappa,z_s,0)\right](\tau), \tag{33}$$

and the $\mathcal{W}_n$'s and $\mathcal{W}_n^{(T)}$'s are the solutions of the following systems of transport equations:

$$\frac{\partial\mathcal{W}_p}{\partial z}+\frac{2p}{\bar{c}(\kappa)}\frac{\partial\mathcal{W}_p}{\partial\tau}=\frac{p^2}{L_{loc}(\omega,\kappa)}\left(\mathcal{W}_{p+1}+\mathcal{W}_{p-1}-2\mathcal{W}_p\right),$$

starting from $\mathcal{W}_p(\tau,\omega,\kappa,z_0,z=z_0)=\mathbf{1}_0(p)\delta(\tau)$, and

$$\frac{\partial\mathcal{W}_p^{(T)}}{\partial z}+\frac{2p}{\bar{c}(\kappa)}\frac{\partial\mathcal{W}_p^{(T)}}{\partial\tau}=\frac{1}{L_{loc}(\omega,\kappa)}\left((p+1)^2\mathcal{W}_{p+1}^{(T)}+p^2\mathcal{W}_{p-1}^{(T)}-(p^2+(p+1)^2)\mathcal{W}_p^{(T)}\right),$$

starting from $\mathcal{W}_p^{(T)}(\tau,\omega,\kappa,z_0,z=z_0)=\mathbf{1}_0(p)\delta(\tau)$. Here the localization length $L_{loc}(\omega,\kappa)$ is defined by

$$L_{loc}(\omega,\kappa)=\frac{4\bar{c}^4}{\gamma\bar{c}(\kappa)^2\omega^2},\qquad \gamma=\int_{-\infty}^{\infty}\mathbb{E}[\nu(0)\nu(z)]dz. \tag{34}$$

Using $|\boldsymbol{\kappa}+\varepsilon\boldsymbol{\lambda}/2|=\kappa+\varepsilon l/2$, $l=\boldsymbol{\kappa}.\boldsymbol{\lambda}/\kappa+O(\varepsilon)$, we get after substitution of (32) into (31) that, in the asymptotic limit $\varepsilon\to 0$,

$$\mathbb{E}\left[u_{TR}^{(3)}(t,\mathbf{x},z)\right] = \frac{1}{(2\pi)^6}\int\int \frac{\bar{c}(\kappa)}{4\bar{c}\sqrt{\bar{I}(\kappa)}}\overline{S_a(\omega,-\boldsymbol{\kappa})}\hat{\bar{G}}_1(h)\hat{G}_2\left(h\boldsymbol{\kappa}+\omega\boldsymbol{\lambda}\right) \quad (35)$$
$$\times\int e^{i\left[h-\omega\boldsymbol{\kappa}.\boldsymbol{\lambda}\bar{c}(\kappa)^2\right]\tau}\mathcal{W}_g^{(-)}\left(\omega,\kappa,\tau\right)d\tau$$
$$\times e^{i\omega(-T+\boldsymbol{\kappa}.\mathbf{X}-\frac{Z}{\bar{c}(\kappa)})}e^{ih\left(t_s+\boldsymbol{\kappa}.\mathbf{x}_s-\frac{z_s}{\bar{c}(\kappa)}\right)+i\omega\left(\boldsymbol{\lambda}.\mathbf{x}_s+\boldsymbol{\lambda}.\boldsymbol{\kappa}\bar{c}(\kappa)z_s\right)}\omega^4 d\omega dh d\boldsymbol{\kappa} d\boldsymbol{\lambda}.$$

Performing the change of variables $\boldsymbol{\lambda}\mapsto\mathbf{k}=\omega\boldsymbol{\lambda}+h\boldsymbol{\kappa}$ and integrating with respect to $\mathbf{k}$ and h, we obtain

$$\mathbb{E}[u_{TR}^{(3)}(t,\mathbf{x},z)] = \frac{1}{(2\pi)^3}\int\int \frac{\bar{c}(\kappa)}{4\bar{c}\sqrt{\bar{I}(\kappa)}}\overline{S_a(\omega,-\boldsymbol{\kappa})}G_1\left(t_s - z_s\frac{\bar{c}(\kappa)}{\bar{c}^2}+\frac{\tau\bar{c}(\kappa)^2}{\bar{c}^2}\right)$$
$$\times G_2\left(\mathbf{x}_s+\boldsymbol{\kappa}\bar{c}(\kappa)z_s-\bar{c}(\kappa)^2\boldsymbol{\kappa}\tau\right)\mathcal{W}_g^{(-)}(\omega,\kappa,\tau)e^{i\omega\left(-T+\boldsymbol{\kappa}.\mathbf{X}-\frac{Z}{\bar{c}(\kappa)}\right)}\omega^2 d\omega d\boldsymbol{\kappa}d\tau.$$

We can deal with the three other components by the same method. In [14] it is also shown that, in the limit $\varepsilon\to 0$, the cross moments of R_g^ε and T_g^ε are zero, so that the contributions of the P_2 and P_4 terms vanish in the limit $\varepsilon\to 0$. Therefore we only need to study the P_1 term which gives

$$\mathbb{E}[u_{TR}^{(1)}(t,\mathbf{x},z)] = -\frac{1}{(2\pi)^3}\int\int \frac{\bar{c}(\kappa)}{4\bar{c}\sqrt{\bar{I}(\kappa)}}\overline{S_b(\omega,-\boldsymbol{\kappa})}G_1\left(t_s - z_s\frac{\bar{c}(\kappa)}{\bar{c}^2}+\frac{\tau\bar{c}(\kappa)^2}{\bar{c}^2}\right)$$
$$\times G_2\left(\mathbf{x}_s+\boldsymbol{\kappa}\bar{c}(\kappa)z_s-\bar{c}(\kappa)^2\boldsymbol{\kappa}\tau\right)\mathcal{W}_g^{(+)}(\omega,\kappa,\tau)e^{i\omega\left(-T+\boldsymbol{\kappa}.\mathbf{X}+\frac{Z}{\bar{c}(\kappa)}\right)}\omega^2 d\omega d\boldsymbol{\kappa}d\tau,$$

where

$$\mathcal{W}_g^{(+)}(\omega,\kappa,\tau) = \sum_{n=0}^{\infty}\left[\mathcal{W}_{n+1}(\cdot,\omega,\kappa,-L,z_s)*\mathcal{W}_n^{(T)}(\cdot,\omega,\kappa,z_s,0)\right](\tau). \quad (36)$$

5.2 Refocusing of the pulse

The main results of this section are the refocusing of the pulse and its self-averaging property. These results are precisely stated in the following theorem which gives the refocusing property and the convergence of the refocused pulse to a deterministic shape concentrated at $-t_s$ in time and at the original source location $(\mathbf{x}_s,z_s)$ in space. We state these results for the longitudinal velocity field, but similar propositions can be stated for the other wave components (transverse velocity and pressure fields).

Theorem 5.1
a) For any $T_0>0$, $R_0>0$, $Z_0>0$, $\delta>0$, and $(t_0,\mathbf{x}_0,z_0)\neq(-t_s,\mathbf{x}_s,z_s)$, we

have

$$\mathbb{P}\left(\sup_{|t-t_0|\leq\varepsilon T_0,|\mathbf{x}-\mathbf{x}_s|\leq\varepsilon R_0,|z-z_0|\leq\varepsilon Z_0}|u_{TR}(t,\mathbf{x},z)|>\delta\right)\stackrel{\varepsilon\to 0}{\longrightarrow}0. \tag{37}$$

where $\mathbb{P}$ *stands for probability.*
b) For any $T_0>0$, $R_0>0$, $Z_0>0$, *and* $\delta>0$, *we have*

$$\mathbb{P}\left(\sup_{|T|\leq T_0,|\mathbf{X}|\leq R_0,|Z|\leq Z_0}|u_{TR}(-t_s+\varepsilon T,\mathbf{x}_s+\varepsilon\mathbf{X},z_s+\varepsilon Z) - U_{TR}(T,\mathbf{X},Z)|>\delta\right)\stackrel{\varepsilon\to 0}{\longrightarrow}0, \tag{38}$$

where U_{TR} *is the deterministic pulse shape*

$$\begin{aligned}&U_{TR}(T,\mathbf{X},Z)=\\&\frac{1}{(2\pi)^3}\int K^+(\omega,\boldsymbol{\kappa})\left[\bar{c}(\kappa)\boldsymbol{\kappa}.\overline{\hat{\mathbf{f}}_{\mathbf{x}}(\omega)}+\overline{\hat{f}_z(\omega)}\right]e^{i\omega\left(-T+\boldsymbol{\kappa}.\mathbf{X}+\frac{Z}{\bar{c}(\kappa)}\right)}\omega^2 d\omega d\boldsymbol{\kappa}\\&+\frac{1}{(2\pi)^3}\int K^-(\omega,\boldsymbol{\kappa})\left[-\bar{c}(\kappa)\boldsymbol{\kappa}.\overline{\hat{\mathbf{f}}_{\mathbf{x}}(\omega)}+\overline{\hat{f}_z(\omega)}\right]e^{i\omega\left(-T+\boldsymbol{\kappa}.\mathbf{X}-\frac{Z}{\bar{c}(\kappa)}\right)}\omega^2 d\omega d\boldsymbol{\kappa}\end{aligned} \tag{39}$$

and the refocusing kernels are given by

$$\begin{aligned}K^{(\pm)}(\omega,\boldsymbol{\kappa})=&\frac{1}{4\bar{c}\bar{\rho}}\int G_1\left(t_s-z_s\frac{\bar{c}(\kappa)}{\bar{c}^2}+\frac{\tau\bar{c}(\kappa)^2}{\bar{c}^2}\right)G_2\left(\mathbf{x}_s+\boldsymbol{\kappa}\bar{c}(\kappa)z_s-\bar{c}(\kappa)^2\boldsymbol{\kappa}\tau\right)\\&\times\mathcal{W}_g^{(\pm)}(\omega,\kappa,\tau)\,d\tau\end{aligned} \tag{40}$$

The proof of the theorem is a generalization of the arguments described in [9,14] and goes along the following main steps.
- We first consider the expected value of u_{TR}. By the result of Section 5.1 we find that this expectation converges to the limiting value given in the theorem.
- We then consider the variance of u_{TR}. We write the second moment as a multiple integral involving the product of four reflection coefficients at four different frequencies. Using the decorrelation property of the reflection coefficient we deduce that the variance goes to zero.
Note that an integral over frequency (ensured by the time domain nature of time reversal) is needed for the stabilization or the self-averaging of the refocused pulse.

The complete expressions of the refocusing densities are complicated and do not allow a simple discussion. In order to be more quantitative we consider the case with $|z_s| \ll L_{loc} \ll L$, and where $L_{loc} = 4\bar{c}^2/(\gamma\omega_0^2)$ is the localization length associated with the carrier wavelength. This means that we address the case of a source embedded in a random half-space at a depth z_s which is not too large so that the wave can penetrate the medium till the depth z_s. We have, up to terms of order $O\left(z_s^2/L_{loc}^2\right)$,

$$
\begin{aligned}
\mathcal{W}_0(\omega,\kappa,\tau,-L,z_s) &= \delta(\tau),\\
\mathcal{W}_1(\omega,\kappa,\tau,-L,z_s) &= \frac{\bar{c}(\kappa)^3}{2\bar{c}^2 L_{loc}} \frac{1}{\left(1+\frac{\bar{c}(\kappa)^3\tau}{2\bar{c}^2 L_{loc}}\right)^2}\mathbf{1}_{[0,\infty)}(\tau),\\
\mathcal{W}_2(\omega,\kappa,\tau,-L,z_s) &= \frac{\bar{c}(\kappa)^6\tau}{2\bar{c}^4 L_{loc}^2} \frac{1}{\left(1+\frac{\bar{c}(\kappa)^3\tau}{2\bar{c}^2 L_{loc}}\right)^3}\mathbf{1}_{[0,\infty)}(\tau),\\
\mathcal{W}_0^{(T)}(\omega,\kappa,\tau,z_s,0) &= \exp\left(-\frac{\bar{c}(\kappa)^2}{\bar{c}^2}\frac{|z_s|}{L_{loc}}\right)\delta(\tau),\\
\mathcal{W}_1^{(T)}(\omega,\kappa,\tau,z_s,0) &= \frac{\bar{c}(\kappa)^3}{2\bar{c}^2 L_{loc}}\mathbf{1}_{[0,2|z_s|/\bar{c}(\kappa)]}(\tau).
\end{aligned}
$$

As a result, from (33) and (36), we deduce the expressions

$$
\mathcal{W}_g^{(+)}(\omega,\kappa,\tau) = \frac{\bar{c}^3(\kappa)}{2\bar{c}^2 L_{loc}} \frac{1}{\left(1+\frac{\bar{c}(\kappa)^3\tau}{2\bar{c}^2 L_{loc}}\right)^2} - \frac{|z_s|}{L_{loc}}\frac{\bar{c}^5(\kappa)}{2\bar{c}^4 L_{loc}} \frac{1-\frac{\bar{c}(\kappa)^3\tau}{2\bar{c}^2 L_{loc}}}{\left(1+\frac{\bar{c}(\kappa)^3\tau}{2\bar{c}^2 L_{loc}}\right)^3}, \quad (41)
$$

$$
\mathcal{W}_g^{(-)}(\omega,\kappa,\tau) = \exp\left(-\frac{\bar{c}(\kappa)^2}{\bar{c}^2}\frac{|z_s|}{L_{loc}}\right)\delta(\tau) + \frac{|z_s|}{L_{loc}}\frac{\bar{c}(\kappa)^5}{2\bar{c}^4 L_{loc}} \frac{1}{\left(1+\frac{\bar{c}(\kappa)^3\tau}{2\bar{c}^2 L_{loc}}\right)^2}. \quad (42)
$$

The first term in the right-hand of (42) corresponds to the contribution of the coherent wave front. The other terms are the contributions of the incoherent waves. Note that the first term in the right-hand side of (41) has a mass of the same order as the contribution of the coherent front.

We parameterize the lateral position of the source by $\mathbf{x}_s = (x_s, 0)$, $x_s > 0$. We assume that the spatial cut-off function associated with the mirror has the form (26). In order to simplify the forthcoming expressions we also assume that $\vec{\mathbf{f}}$ is given by (25) where ω_0 is the high-carrier frequency and T_w is the time pulse width, with $\omega_0 T_w \gg 1$.

Refocusing of the front. Let us assume that we record only the coherent front. This means that the support of the function G_1 is of the form $[T_0 -$

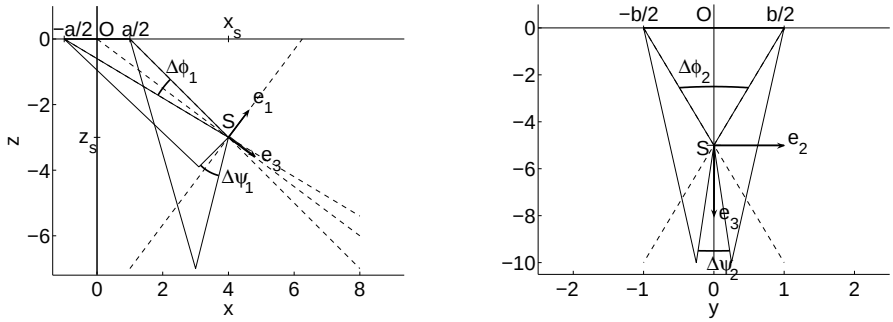

Fig. 7. Cones of aperture $(\Delta\phi_1, \Delta\phi_2)$ and $(\Delta\Psi_1, \Delta\Psi_2)$ generated respectively by the coherent wave front and by the incoherent multiply scattered waves $((\vec{\mathbf{e}}_1, \vec{\mathbf{e}}_3)$-section on the left and $(\vec{\mathbf{e}}_2, \vec{\mathbf{e}}_3)$-section on the right).

$\delta, T_0 + \delta]$ with $\varepsilon \ll \delta \ll 1$ and

$$T_0 = \frac{OS}{\bar{c}} + t_s$$

corresponds to the arrival time at the mirror of the front wave emitted by the source. Then the form of the focal spot normalized by the maximal amplitude of the focal spot obtained in the homogeneous case is

$$U_{TR}(T, \mathbf{X}, Z) \simeq \exp\left(-\frac{OS^2}{|z_s| L_{loc}}\right) \frac{\vec{\mathbf{OS}}}{OS}.\vec{\mathbf{f}}_0 \left(-\frac{T}{T_w} + \frac{(\mathbf{X}, Z).\vec{\mathbf{e}}_3}{\bar{c} T_w}\right) \times \hat{g}_2 \left(\frac{\omega_0 \Delta\phi_1}{\bar{c}}(\mathbf{X}, Z).\vec{\mathbf{e}}_1, \frac{\omega_0 \Delta\phi_2}{\bar{c}}(\mathbf{X}, Z).\vec{\mathbf{e}}_2\right) \tag{43}$$

where the $\Delta\phi_j$'s are defined by (28-29). This shows that the focal spot shape is the same as in the homogeneous case. The only difference is a slight reduction of the amplitude due to the decay of the coherent energy.

Now, let us assume that we record some part of the long multiply scattered incoherent waves. This means that $G_1(t) = \mathbf{1}_{[T_1, T_2]}(t)$ where $T_0 < T_1 < T_2$.

Refocusing of the coda for a mirror not above the source. We assume that the mirror is not exactly above the source and denote by $x_s > 0$ the offset. The expression for the refocused field U_{TR} can be significantly simplified if we assume that the four following hypotheses are satisfied:

H_1. The time window cut-off function is of the form $G_1(\tau) = \mathbf{1}_{[T_1, T_2]}(\tau)$ with $T_2 > T_1 > T_0$, where $T_0 = t_s + OS/\bar{c}$ is the arrival time of the front. This means that we do not capture the coherent front.

H_2. The spatial shape of the time-reversal mirror is of the form $G_2(\mathbf{x}) = g_2(x/a, y/b)$, the reference frame is oriented such that the source location is $\mathbf{x}_s = (x_s, 0)$, and the offset x_s is much larger than the mirror diameter

$\sqrt{a^2+b^2}$. This means that we consider a narrow-aperture situation.

H_3. The source emits a pulse with a carrier frequency ω_0 that is much larger than the bandwidth $1/T_w$ (equal to the inverse of the pulse width). This allows us to derive a simplified high-frequency expression for the refocused field.

H_4. The random slab is a semi-infinite random half-space and the source depth is much smaller than the localization length $L_{loc} = 4\bar{c}^2/(\gamma\omega_0^2)$, with ω_0 the carrier frequency. This allows us to obtain explicit approximations for the kernel densities $\mathcal{W}_g$, which in turn will allow us to discuss quantitatively the properties of the refocusing.

We introduce the angles $0 < \theta_1 < \theta_2 < \pi/2$:

$$\theta_j = \arccos\left(\frac{x_s}{\bar{c}(T_j - t_s)}\right) \tag{44}$$

As discussed below and shown in Figure 7, this defines a "temporal" cone delimited by the angle of the shortest ray θ_1 and the angle of the longest ray θ_2 recorded by the center point of the mirror. After some algebra we obtain that the refocused focal spot is:

$$\begin{aligned}|U_{TR}(T,\mathbf{X},Z)| = \frac{ab\omega_0^2}{32\pi^2\bar{\rho}\bar{c}^3 x_s L_{loc}} \Bigg| \int_{\cos(\theta_2)}^{\cos(\theta_1)} \frac{1}{\left(1+\frac{x_s}{2L_{loc}s\sqrt{1-s^2}}\right)^2} \frac{1}{\sqrt{1-s^2}} \\ \times \hat{g}_2\left(\frac{\omega_0 as}{\bar{c}x_s}(X - \frac{s}{\sqrt{1-s^2}}Z), \frac{\omega_0 bs}{\bar{c}x_s}Y\right) e^{i\frac{\omega_0}{\bar{c}}\left(sX+Z\sqrt{1-s^2}-T\right)} \\ \times \left[f_{0z} + \frac{s}{\sqrt{1-s^2}}f_{0x}\right]\left(-\frac{T}{T_w} + \frac{Xs+Z\sqrt{1-s^2}}{\bar{c}T_w}\right) ds\Bigg|\end{aligned} \tag{45}$$

The y-component f_{0y} of the source does not appear in this leading-order expression, because it has not been recorded by the mirror due to the fact that the source location has a zero y-coordinate. As pointed out above, this expression holds true if $|z_s| \ll L_{loc}$ and $x_s > 0$. If moreover $x_s \ll L_{loc}$, then the first factor in the integral can be simplified to one. Let us write $\theta_1 = \bar{\theta} - \Delta\theta/2$ and $\theta_2 = \bar{\theta} + \Delta\theta/2$, with

$$\bar{\theta} = \frac{\theta_1+\theta_2}{2} = \frac{1}{2}\left[\arccos\left(\frac{x_s}{\bar{c}(T_2-t_s)}\right) + \arccos\left(\frac{x_s}{\bar{c}(T_1-t_s)}\right)\right].$$

We now introduce the new orthonormal frame $(\vec{\mathbf{w}}_1, \vec{\mathbf{w}}_2, \vec{\mathbf{w}}_3)$ defined by

$$\vec{\mathbf{w}}_1 = \begin{pmatrix}\sin\bar{\theta}\\0\\-\cos\bar{\theta}\end{pmatrix}, \quad \vec{\mathbf{w}}_2 = \begin{pmatrix}0\\1\\0\end{pmatrix}, \quad \vec{\mathbf{w}}_3 = \begin{pmatrix}\cos\bar{\theta}\\0\\\sin\bar{\theta}\end{pmatrix},$$

and described in the right picture of Figure 9. In this frame, $\vec{\mathbf{w}}_3$ is the main direction of arrival of the time-reversed incoherent waves which have interacted with the medium below z_s and which participate to the refocusing at the original source location. Note the striking difference with the direction of arrival $\vec{\mathbf{e}}_3$ of the time-reversed front (compare the two pictures in Figure 9). The range of $\bar{\theta}$ is $(\theta_0, \pi/2)$ with $\theta_0 = \arccos(x_s/OS)$: $\bar{\theta}$ is close to θ_0 when $T_0 < T_1 < T_2 \searrow T_0$, corresponding to the recording and re-emission of a short piece of incoherent waves near the front. The angle $\bar{\theta}$ is close to $\pi/2$ when $T_2 > T_1 \nearrow \infty$, corresponding to a piece of incoherent waves far from the front.

We can simplify further the expression (45) by assuming that $\Delta\theta$ is relatively small so that we can expand the arguments of the integral in $s \in (\cos(\bar{\theta} - \Delta\theta/2), \cos(\bar{\theta} + \Delta\theta/2))$ around the central value $\cos(\bar{\theta})$. We then obtain that, in the frame $(\vec{\mathbf{w}}_1, \vec{\mathbf{w}}_2, \vec{\mathbf{w}}_3)$, the envelope of the refocused field (45) can be approximated as

$$|U_{TR}(T, \mathbf{X}, Z)| \simeq \left|\hat{g}_2\left(\frac{\omega_0 \Delta\Psi_1}{\bar{c}}(\mathbf{X}, Z).\vec{\mathbf{w}}_1, \frac{\omega_0 \Delta\Psi_2}{\bar{c}}(\mathbf{X}, Z).\vec{\mathbf{w}}_2\right)\right| \left|\mathrm{sinc}\left(\frac{\omega_0 \Delta\theta}{2\bar{c}}(\mathbf{X}, Z).\vec{\mathbf{w}}_1\right)\right| \times \left|\vec{\mathbf{w}}_3.\vec{\mathbf{f}}_0\left(-\frac{T}{T_w} + \frac{(\mathbf{X}, Z).\vec{\mathbf{w}}_3}{\bar{c}T_w}\right)\right|. \quad (46)$$

where

$$\Delta\Psi_1 = \frac{a}{x_s \tan\bar{\theta}}, \qquad \Delta\Psi_2 = \frac{b\cos\bar{\theta}}{x_s}$$

a) In the $\vec{\mathbf{w}}_3$-direction, the focal spot size is imposed by the initial pulse width T_w and it is given by $\bar{c}T_w$.

b) In the $\vec{\mathbf{w}}_2$-direction, the focal spot is determined by the mirror size b and it has the size $\lambda_0/\Delta\Psi_2$ where $\Delta\Psi_2 = b(\cos\bar{\theta})/x_s$ ($\Delta\Psi_2$ is represented in the right picture of Figure 7). This size is consistent with the Rayleigh formula. The random medium cannot help refocusing in this transverse direction because no scattering occurs in this direction. This is connected to the layered structure of the medium and should not happen in a real three-dimensional random medium.

c) In the $\vec{\mathbf{w}}_1$-direction, the focal spot radius depends on the two angular cones $\Delta\theta$ and $\Delta\Psi_1$, which can be chosen independently:
- The angle $\Delta\theta$ is determined by the recording time interval $[T_1, T_2]$:

$$\Delta\theta = \arccos\left(\frac{x_s}{\bar{c}(T_2 - t_s)}\right) - \arccos\left(\frac{x_s}{\bar{c}(T_1 - t_s)}\right)$$

This "temporal" cone is delimited by the angle of the shortest ray and the

angle of the longest ray recorded by the center point of the mirror.
- The angle $\Delta\Psi_1$ is determined by the spatial size a of the mirror. This "geometrical" cone is delimited by the two rays with the same travel time $x_s/[\bar{c}\cos(\bar{\theta})]$ originating from the two ends of the mirror, at $x = -a/2$ and $x = a/2$. These ays are plotted in the left picture of Figure 7. The value of the angle $\Delta\Psi_1$ is computed by trigonometry. The cross-over of these two rays is responsible for the minus sign in the first argument of $\hat{g}_2$ in (46).

Two cases can be then distinguished.

1) If $\Delta\theta \ll \Delta\Psi_1 \ll 1$, which is the case in particular if only a very short piece of coda is recorded, then Eq. (45) can be simplified into

$$|U_{TR}(T,\mathbf{X},Z)| \simeq \left|\hat{g}_2\left(\frac{\omega_0\Delta\Psi_1}{\bar{c}}(\mathbf{X},Z).\vec{\mathbf{w}}_1, \frac{\omega_0\Delta\Psi_2}{\bar{c}}(\mathbf{X},Z).\vec{\mathbf{w}}_2\right)\right| \times \left|\vec{\mathbf{w}}_3.\vec{\mathbf{f}}_0\left(-\frac{T}{T_w} + \frac{(\mathbf{X},Z).\vec{\mathbf{w}}_3}{\bar{c}T_w}\right)\right| \tag{47}$$

In this case, the angular diversity of the refocused waves mainly originates from the numerical aperture of the mirror, and we get a formula in qualitative agreement with the Rayleigh resolution formula. More quantitatively, if we record a piece of the coda just after the front, meaning that T_1, T_2 are close to T_0, then $\bar{\theta} = \arccos(x_s/OS)$ and the focal spot size is $\lambda_0|z_s|/a$. Recall that the focal spot size generated by the front is given by $\lambda_0 OS^2/(a|z_s|)$. This shows that the random medium gives a **compensation for the offset** x_s.

2) If $\Delta\Psi_1 \ll \Delta\theta \ll 1$, then Eq. (45) can be simplified into

$$|U_{TR}(T,\mathbf{X},Z)| \simeq \left|\hat{g}_2\left(0, \frac{\omega_0\Delta\Psi_2}{\bar{c}}(\mathbf{X},Z).\vec{\mathbf{w}}_2\right)\right| \left|\mathrm{sinc}\left(\frac{\omega_0\Delta\theta}{2\bar{c}}(\mathbf{X},Z).\vec{\mathbf{w}}_1\right)\right| \times \left|\vec{\mathbf{w}}_3.\vec{\mathbf{f}}_0\left(-\frac{T}{T_w} + \frac{(\mathbf{X},Z).\vec{\mathbf{w}}_3}{\bar{c}T_w}\right)\right| \tag{48}$$

In this case, the angular diversity of the refocused waves mainly originates from the temporal refocusing cone $\Delta\theta$ described above. Therefore the focal spot size is $\lambda_0/\Delta\theta$ as soon as $\Delta\theta > a/OS$. This size is determined by the angular diversity of the refocused incoherent waves and it is much smaller than the prediction of the Rayleigh resolution formula. As we show below, (48) can be extended to $\Delta\theta \sim 1$. The focal spot size is then of the order of the **diffraction limit** if $\Delta\theta \sim 1$, that is, if $T_2 - T_1 \geq \bar{c}/x_s$. This means that recording a long coda allows us to enhance dramatically the **effective aperture** of the mirror thanks to the multiple scattering in the random medium below the source. The spot shape is plotted in Figure 10. Qualitatively, if we increase the recording time window by taking a larger T_2 and a smaller T_1, then we get a wider and

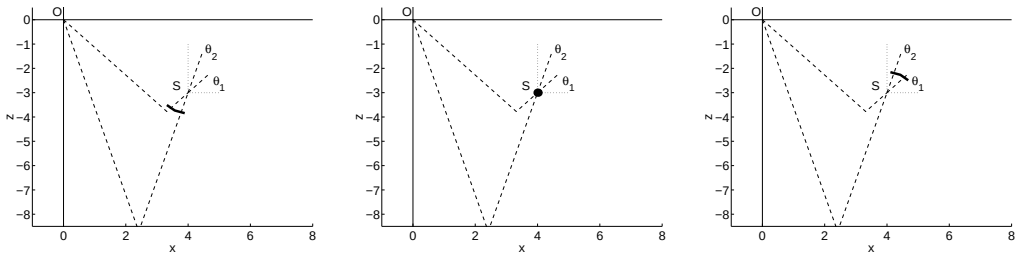

$t < -t_s$ $\qquad$ $t = -t_s$ $\qquad$ $t > -t_s$

Fig. 8. Pulse refocusing when the incoherent waves are recorded.

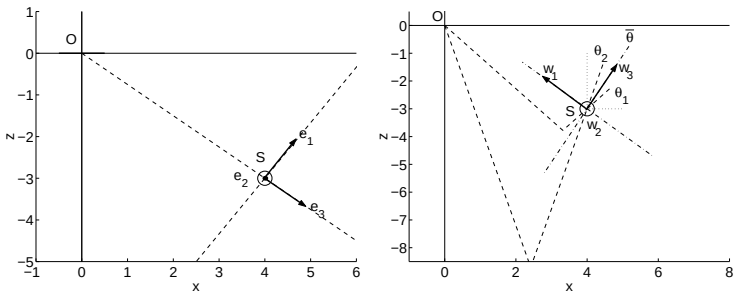

Fig. 9. Frame adapted to the refocusing of the front wave (left picture) and frame adapted to the refocusing of the incoherent waves (right picture).

wider numerical aperture. The largest numerical aperture is $[\theta_0, \pi/2]$ where $\theta_0 = \arccos(x_s/OS)$. It is obtained for T_1 close to T_0 and $T_2 - T_0 \gg \bar{c}/x_s$.

In the case where $\Delta\psi_1 \ll \Delta\theta \sim 1$, we can re-consider the expression (45) and focus our attention on the spatial profile in the $\vec{\mathbf{w}}_1$-direction. We obtain that, for any r,

$$|U_{TR}(T=0,(\mathbf{X},Z)=r\vec{\mathbf{w}}_1)| \simeq \left| \int_{-1/2}^{1/2} \cos\left(\frac{\omega_0 r}{\bar{c}}\cos(\Delta\theta\xi)\right) d\xi \right| ,$$

which shows that the size of the focal spot is of the order of the carrier wavelength λ_0 when $\Delta\theta \sim 1$. If $\Delta\theta$ could become close to 2π, then the focal spot would converge to the Bessel function $J_0(\omega_0 r/\bar{c})$ and its radius would be equal to $0.383\lambda_0$.

Note that in the regime $|z_s| \ll L_{loc}$ studied in this section the incoherent waves scattered by the random slab $(z_s, 0)$ do not contribute to the refocusing at the original source location.

Let us finally comment on the case where $|z_s| \geq L_{loc}$. If z_s is large and becomes comparable to the localization length, then the refocusing can be even better, but it is more cumbersome to write explicitly closed-form formulas (no analytical expressions are available for the refocusing densities). Qualitatively, waves

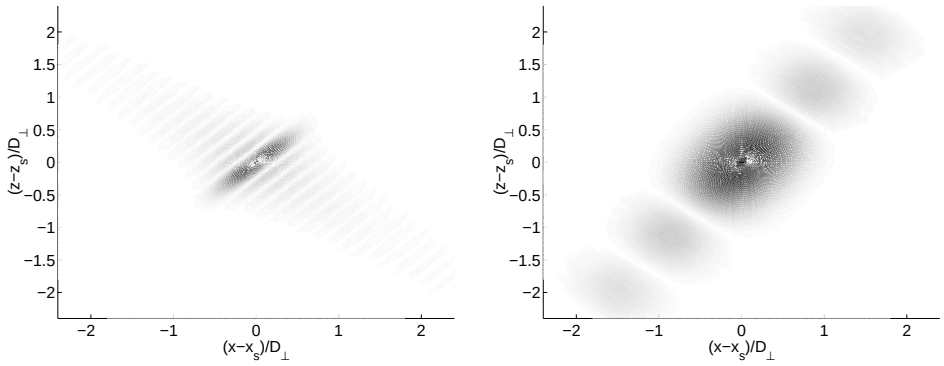

Fig. 10. Left picture: Pulse shape generated by the refocusing of the incoherent waves in the plane $(\vec{\mathbf{w}}_1, \vec{\mathbf{w}}_3)$. The mirror is square with size a and the initial pulse profile is Gaussian with duration T_w. Here $a = b = 0.33$, $z_s = -3$, $x_s = 4$ ($OS = 5$), $t_s = 0$ ($\bar{c}T_0 = 5$), $\bar{c}T_1 = 6$, $\bar{c}T_2 = 8$ so that $\tan\bar{\theta} = 1.38$, $\Delta\phi_1 = 0.04$, $\Delta\Psi_1 = 0.06$ and $\Delta\theta = 0.2$. As a result the spot shape is a sinc function with radius $D_\perp/5$ where $D_\perp = \lambda_0 x_s \tan\bar{\theta}/a$ in the $\vec{\mathbf{w}}_1$ direction and a Gaussian function with radius $\bar{c}T_w$ in the $\vec{\mathbf{w}}_3$ direction. The spot shape in the $\vec{\mathbf{w}}_2$ direction is a sinc function with radius $\lambda_0/\Delta\Psi_2$ where $\Delta\Psi_2 = b\cos\bar{\theta}/x_s$. For comparison we show the focal spot in the homogeneous case in the right picture.

scattered in the slab $[z_s, 0]$ can contribute to the pulse refocusing of the pulse. Under the best conditions (where the emitted wave is completely recorded) the numerical aperture is generated by two cones $(\theta_0, \pi/2)$ and $(-\pi/2, -\theta_0)$.

Refocusing of the coda for a mirror above the source. We now address the case where the mirror is located above the source: $x_s = 0$. If we assume the set of hypotheses H_1-H_4 stated above (except the requirement $x_s \gg \sqrt{a^2+b^2}$), then, by integrating (40) we obtain, to leading order in $|z_s|/L_{loc}$:

$$U_{TR}(T, \mathbf{X}, Z) = \frac{ab\omega_0^2}{16\pi\bar{\rho}\bar{c}^3 L_{loc}|z_s|} f_{0z}\left(-\frac{T}{T_w} + \frac{Z}{\bar{c}T_w}\right) e^{i\omega_0(-T+\frac{Z}{\bar{c}})} \times \int_{q_2}^{q_1} \hat{g}_2\left(\frac{\omega_0 a}{\bar{c}|z_s|}qX, \frac{\omega_0 b}{\bar{c}|z_s|}qY\right) dq$$

where the parameters $0 < q_2 < q_1 < 1$ are given by

$$q_j = \left(1 + \frac{\bar{c}(T_j - T_0)}{|z_s|}\right)^{-1}$$

Here $T_2 > T_1 > T_0$, which means that the parameters q_j's are smaller than one. The spatial profile of the refocused field has therefore a radius which is larger than the Rayleigh limit. In the case where the mirror is located just above the source, the refocusing of the incoherent waves cannot involve super-resolution, because the angular diversity of the refocused waves is very small

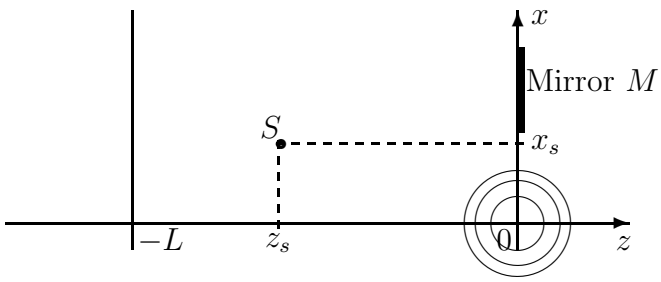

Fig. 11. Emission from a point source located at $O = (\mathbf{0}, 0)$. The scatterer position is $S = (\mathbf{x}_s, z_s)$. The signal is recorded at the mirror M.

(the geometry is as in the right picture of Figure 7 with the cone of aperture $\Delta\Psi_2 = q_1 b/|z_s|$).

6 Time reversal with a passive scatterer

The analysis we have carried out for an active source can be extended to the case where a passive scatterer embedded in a random medium is illuminated by a source located at the surface. We describe briefly how our active source results also apply to this passive scattering case. In this case the time reversal mirror records the scattered signal, where the scattering results from both the interaction of the wave field with the small inhomogeneities and with the embedded scatterer. The mirror is modeled exactly as above, that is, it has a large spatial extent and records a long time segment of the wave field which it sends back into the medium after time reversal. We will show that again the time reversed wave field focuses tightly on the scatterer and that a super resolution effect can be observed.

The random medium occupying the slab $(-L, 0)$ is defined as in previous sections. Now a point source is located just above the surface at $(\mathbf{0}, 0^+)$ and emits at time zero a short pulse, moreover, a scatterer is buried inside of the random medium. The wave propagation is again described by (1) with the external source given as in (3):

$$\vec{\mathbf{F}}(t, \mathbf{x}, z) = \varepsilon^2 \begin{bmatrix} \mathbf{0} \\ 1 \end{bmatrix} f\left(\frac{t}{\varepsilon}\right) \delta(\mathbf{x})\, \delta(z)\,, \tag{49}$$

and scaled so that it will produce a refocused field of order one. Figure 11 illustrates the geometry in the situation: a point source is located at the origin $O = (\mathbf{0}, 0)$, the scatterer position is $S = (\mathbf{x}_s, z_s)$, and the time reversal mirror M is located in the plane $z = 0$, but not necessarily at the origin O. We model the scatterer as a local change in the density of the medium:

$$\rho(\mathbf{x}, z) = \bar{\rho} + \rho_1 \mathbf{1}_B(\mathbf{x}, z),$$

where B is a small domain around $S = (\mathbf{x}_s, z_s)$. The system that governs the propagation of the acoustic waves can be written

$$\bar{\rho}\frac{\partial \vec{\mathbf{u}}}{\partial t} + \vec{\nabla} p = \vec{\mathbf{F}} - \rho_1 \mathbf{1}_B(\mathbf{x}, z)\frac{\partial \vec{\mathbf{u}}}{\partial t}, \qquad \frac{1}{K(z)}\frac{\partial p}{\partial t} + \nabla.\vec{\mathbf{u}} = 0.$$

We apply the **Born approximation** for the modeling of the scattering by S [18]: the total field at the surface is the superposition of the primary field $(\vec{\mathbf{u}}_0, p_0)$ which solves the problem

$$\bar{\rho}\frac{\partial \vec{\mathbf{u}}_0}{\partial t} + \vec{\nabla} p_0 = \vec{\mathbf{F}}, \qquad \frac{1}{K(z)}\frac{\partial p_0}{\partial t} + \nabla.\vec{\mathbf{u}}_0 = 0\,,$$

and of a secondary field $(\vec{\mathbf{u}}_1, p_1)$ which is due to the emission of a secondary source located at S. The emission of the secondary source is proportional to the primary field at the position of the scatterer:

$$\bar{\rho}\frac{\partial \vec{\mathbf{u}}_1}{\partial t} + \nabla p_1 = -\rho_1 \mathbf{1}_B(\mathbf{x}, z)\frac{\partial \vec{\mathbf{u}}_0}{\partial t}, \qquad \frac{1}{K(z)}\frac{\partial p_1}{\partial t} + \vec{\nabla}.\vec{\mathbf{u}}_1 = 0.$$

We assume that the scattering region B is smaller than the wavelength, and we model it by a point scatterer with **scattering volume** $\varepsilon^3\sigma_s$ where the scale factor ε^3 is imposed by the wavelength scaling ε, and σ_s is small so that the Born approximation is valid:

$$\rho_1 \mathbf{1}_B(\mathbf{x}, z) = \varepsilon^3 \bar{\rho}\sigma_s \delta(\mathbf{x} - \mathbf{x}_s)\delta(z - z_s)\,. \tag{50}$$

The total field is decomposed as $\vec{\mathbf{u}} = \vec{\mathbf{u}}_0 + \vec{\mathbf{u}}_1$, $p = p_0 + p_1$. Next we take a Fourier transform with respect to the time and the transverse spatial variables and, using the generalized reflection and transmission coefficients to express the primary field and the form (50) for the scatterer, we find that the secondary field $(\vec{\mathbf{u}}_1, p_1)$ solves the problem

$$-\bar{\rho}\frac{i\omega}{\varepsilon}\hat{\mathbf{v}}_1 + i\frac{\omega}{\varepsilon}\boldsymbol{\kappa}\hat{p}_1 = \varepsilon^3 \mathbf{S}_{1,\mathbf{x}}(\omega)e^{-i\frac{\omega}{\varepsilon}\boldsymbol{\kappa}.\mathbf{x}_s}\delta(z - z_s), \tag{51}$$

$$-\bar{\rho}\frac{i\omega}{\varepsilon}\hat{u}_1 + \frac{\partial \hat{p}_1}{\partial z} = \varepsilon^3 S_{1,z}(\omega)e^{-i\frac{\omega}{\varepsilon}\boldsymbol{\kappa}.\mathbf{x}_s}\delta(z - z_s), \tag{52}$$

$$-\frac{1}{K(z)}\frac{i\omega}{\varepsilon}\hat{p}_1 + i\frac{\omega}{\varepsilon}\boldsymbol{\kappa}.\hat{\mathbf{v}}_1 + \frac{\partial \hat{u}_1}{\partial z} = 0,$$

where $\vec{\mathbf{u}}_1 = (\mathbf{v}_1, u_1)$, $\vec{\mathbf{u}}_0 = (\mathbf{v}_0, u_0)$, and the secondary source terms given by

$$\mathbf{S}_{1,\mathbf{x}}(\omega) = \frac{i\sigma_s}{(2\pi)^2}\int \frac{\boldsymbol{\kappa}'}{2}\Big[R_g(\omega, \kappa', z_s)e^{i\frac{\omega}{\varepsilon}(\boldsymbol{\kappa}'.\mathbf{x}_s + z_s/\bar{c}(\kappa'))} - T_g(\omega, \kappa', z_s)e^{i\frac{\omega}{\varepsilon}(\boldsymbol{\kappa}'.\mathbf{x}_s - z_s/\bar{c}(\kappa'))}\Big]\hat{f}(\omega)\omega^3 d\boldsymbol{\kappa}', \tag{53}$$

$$S_{1,z}(\omega) = \frac{i\sigma_s}{(2\pi)^2} \int \frac{\bar{\rho}}{2\bar{\zeta}(\kappa')} \Big[R_g(\omega, \kappa', z_s) e^{i\frac{\omega}{\varepsilon}(\boldsymbol{\kappa}'.\mathbf{x}_s + z_s/\bar{c}(\kappa'))} + T_g(\omega, \kappa', z_s) e^{i\frac{\omega}{\varepsilon}(\boldsymbol{\kappa}'.\mathbf{x}_s - z_s/\bar{c}(\kappa'))} \Big] \hat{f}(\omega)\omega^3 d\boldsymbol{\kappa}'. \tag{54}$$

These source terms correspond to the emission from a point source similar to the embedded source problem discussed in Section 3. Making the substitutions

$$t_s \mapsto 0\,, \qquad \hat{\mathbf{f}}_{\mathbf{x}}(\omega) \mapsto \mathbf{S}_{1,\mathbf{x}}(\omega)\,, \qquad \hat{f}_z(\omega) \mapsto S_{1,z}(\omega),$$

in (14), we can proceed as in the case with an internal source.

We now record the signal at the mirror after the direct arrival from the source. The recorded field is made of three components:
- The incoherent primary waves which are of amplitude $\varepsilon^{3/2}$ [1].
- The coherent secondary field. Indeed, the front pulse emitted by the source O has been scattered by S. This has created a secondary coherent source proportional to $\sigma_S \varepsilon^3$. It therefore generates a new coherent front of amplitude $\sigma_s \varepsilon^2$.
- The incoherent secondary waves, which are of amplitude $\sigma_s \varepsilon^{5/2}$.

Next we time reverse the recorded signal and we amplify it by a factor $1/\varepsilon$ before re-emission so that the secondary coherent source appears as proportional to $\sigma_s \varepsilon^2$. Therefore we create a refocusing spot at the scatterer S of amplitude σ_s using the results of the previous section. Note also that refocusing at the original source location O takes place at a later time, with a large amplitude of order $1/\varepsilon$. Also, the background incoherent field generated by the re-emission is of small amplitude, of the order of $\varepsilon^{1/2}$.

The description of the super resolution at the location of the scatterer S is similar to the one given in the previous section. The differences come from the propagation of the front wave from the source O to the scatterer S, which creates a small random time-shift and a deterministic spreading of the secondary source. These two differences are not compensated by time reversal in the refocusing at S. They are quantitatively described by the O'Doherty-Anstey theory [8,20].

More precisely, for any $T_0 > 0$, $R_0 > 0$, $Z_0 > 0$, and $\delta > 0$, we have

$$\mathbb{P}\left(\sup_{|T|\le T_0, |\mathbf{X}|\le R_0, |Z|\le Z_0} \left| u_{TR}\left(-\frac{OS}{\bar{c}} + \varepsilon T, \mathbf{x}_s + \varepsilon \mathbf{X}, z_s + \varepsilon Z \right) - U_{TR}(T + \chi_c, \mathbf{X}, Z) \right| > \delta \right) \stackrel{\varepsilon \to 0}{\longrightarrow} 0. \tag{55}$$

The random travel time correction χ_c is a zero-mean Gaussian random variable

with variance $\gamma OS/(4\bar{c}^2)$. The deterministic refocused pulse shape is of the form (39). Here the refocusing kernels are given by

$$K^{\pm}(\omega,\boldsymbol{\kappa}) = \int G_1\left(\frac{OS}{\bar{c}} - z_s\frac{\bar{c}(\kappa)}{\bar{c}^2} + \tau\right) G_2\left(\mathbf{x}_s + \boldsymbol{\kappa}\bar{c}(\kappa)z_s - \bar{c}^2\boldsymbol{\kappa}\tau\right) \times \mathcal{W}_g^{(\pm)}(\omega,\kappa,\tau)\, d\tau \left(\frac{\sigma_s|z_s|\omega^2}{16\pi\bar{c}^3\bar{\rho}OS^3} e^{-\frac{|z_s|}{2L_{loc}(\omega)}}\right) \tag{56}$$

where $1/L_{loc}(\omega) = (\omega^2\gamma OS)/(4|z_s|\bar{c}^2)$. If we compare the expression (56) of the refocusing kernels in the embedded scatterer problem with the equivalent expressions (40) in the internal source problem, we find that the principal super resolution effect will be as in the case with an internal source up to a spreading by a Gaussian kernel. Note however that the statistically stable refocused wave field is observed at the randomly corrected 'fine-scale' time $T + \chi_c$.

We will skip the technical details of the proof, but remark that the main difference with the proof given in the case of an active source is the appearance of a third transmission/reflection coefficient factor modeling the propagation from O to S. The moment analysis shows that only the coherent part of this factor gives a significant contribution to the refocused shape, and this coherent part is described by the ODA theory.

Note finally that, in the situation described in this section, the time-reversal mirror receives a very-low amplitude signal, of order $\varepsilon^{3/2}$, it amplifies the received signal by the factor ε^{-1}, so that it sends back an acoustic signal whose amplitude is small, of order $\varepsilon^{1/2}$. This generates a focal spot at the location of the scatterer whose amplitude is of order one. However, the time-reversal mirror could send back a signal with amplitude of order one, which means that it could amplify the received signal by the factor $\varepsilon^{-3/2}$. If the time-reversal experiment is performed with this amplification factor, then a very high amplitude, of order $\varepsilon^{-1/2}$, is obtained at the location of the scatterer.

To summarize this section, we have shown that, by time reversing multiply scattered incoherent waves, it is possible to concentrate energy on a passive scatterer buried in a random medium. The amplification of these time reversed waves is the basic principle of time-reversal ultrasound target destruction, applied for instance to kidney stones [12]. The iteration of this procedure can be used to enhance the refocusing at the selected target, as described in [21,23–25]. In such experiments, both sides of the medium surrounding the target are accessible, and the addition of a randomly layered slab below the medium (opposite to the source and time-reversal mirror apparatus) can dramatically enhance the refocusing at the target according to the theory developed in this section. The randomly layered slab can be produced once for all due to the

statistical stability, with a correlation length compatible with the source and the regime of separation of scales studied in this paper.

7 Conclusion

In this paper we have studied time reversal in three-dimensional randomly layered media. We have considered the case of a point source inside of the medium emitting a short pulse and a time reversal mirror recording the transmitted waves at the surface of the medium. We have shown that, after time reversal, the re-propagated waves refocus at the location of the source. We have given a detailed analysis of the properties of this refocusing in a regime of separation of scales, and, in particular, we have deduced effective aperture enhancement and super resolution effects due to the multipathing of waves which have traveled below the source and have been recorded and sent back by the mirror. Finally we have proposed an application to the problem of improving the focusing on a scatterer buried in a random medium.

Acknowledgements

This work was supported by ONR grants N00014-02-1-0089 and N00014-05-1-0442. J. Garnier was supported by the program ACI-NIM-2003-94. K Sølna was supported by NSF grant DMS0307011 and the Sloan Foundation.

References

[1] M. Asch, W. Kohler, G. Papanicolaou, M. Postel, and B. White, Frequency content of randomly scattered signals, SIAM Rev. 33 (1991) 519-625.

[2] G. Bal, G. Papanicolaou, and L. Ryzhik, Self-averaging in time reversal for the parabolic wave equation, Stochastics and Dynamics 2 (2002) 507-531.

[3] G. Bal and L. Ryzhik, Time reversal and refocusing in random media, SIAM J. Appl. Math 63 (2003)1475-1498.

[4] P. Blomgren, G. Papanicolaou, and H. Zhao, Super-resolution in time-reversal acoustics, J. Acoust. Soc. Am. 111 (2002) 230-248.

[5] L. Borcea, G. Papanicolaou, and C. Tsogka, Theory and applications of time reversal and interferometric imaging, Inverse Problems **19**:S (2003) 134-164.

[6] L. Borcea, G. Papanicolaou, and C. Tsogka, Coherent interferometry in finely layered random media, preprint.

[7] M. Born and E. Wolf, *Principles of optics*, Cambridge University Press, Cambridge, 1999

[8] J. Chillan and J.-P. Fouque, Pressure fields generated by acoustical pulses propagating in randomly layered media, SIAM J. Appl. Math. 58 (1998) 1532-1546.

[9] J.-F. Clouet and J.-P. Fouque, A time-reversal method for an acoustical pulse propagating in randomly layered media, Wave Motion 25 (1997) 361-368.

[10] A. Derode, P. Roux, and M. Fink, Robust acoustic time-reversal with high-order multiple scattering, Phys. Rev. Lett. 75 (1995) 4206-4209.

[11] A. Derode, A. Tourin, J. de Rosny, M. Tanter, S. Yon, and M. Fink, Taking advantage of multiple scattering to communicate with time reversal antennas, Phys. Rev. Lett. 90 (2003) 014301.

[12] M. Fink, Time reversed acoustics, Scientific American (November 1999) 91-97.

[13] M. Fink, G. Montaldo, and M. Tanter, Time reversal acoustics in biomedical engineering, Annual Review of Biomedical Engineering 5 (2003) 465-497.

[14] J.-P. Fouque, J. Garnier, A. Nachbin, and K. Sølna, Time reversal refocusing for point source in randomly layered media, Wave Motion 42 (2005) 238-260.

[15] J.-P. Fouque and K. Sølna, Time-reversal aperture enhancement, SIAM Multiscale Modeling and Simulation 1 (2003) 239-259.

[16] J. Garnier, Imaging in randomly layered media by cross-correlating noisy signals, SIAM Multiscale Modeling and Simulation 4 (2005) 610-640.

[17] D. R. Jackson and D. R. Dowling, Phase-conjugation in underwater acoustics, J. Acoust. Soc. Am. 89 (1991) 171-181.

[18] P. M. Morse and K. U. Ingard, *Theoretical acoustics*, McGraw-Hill, New York, 1968.

[19] G. Papanicolaou, L. Ryzhik, and K. Sølna, Statistical stability in time reversal, SIAM J. Appl. Math. 64 (2004) 1133-1155.

[20] G. Papanicolaou and K. Sølna, Ray theory for a locally layered random medium, Waves Random Media 10 (2000) 151-198.

[21] C. Prada and M. Fink, Eigenmodes of the time reversal operator: A solution to selective focusing in multiple-target media, Wave Motion 20 (1994) 151-163.

[22] C. Prada, E. Kerbrat, D. Cassereau, and M. Fink, Time reversal techniques in ultrasonic nondestructive testing of scattering media, Inverse Problems 18 (2002) 1761-1773.

[23] C. Prada, S. Manneville, D. Spolianski, and M. Fink, Decomposition of the time reversal operator: Detection and selective focusing on two scatterers, J. Acoust. Soc. Am. 99 (1996) 2067-2076.

[24] C. Prada, J.-L. Thomas, and M. Fink, The iterative time reversal mirror: Analysis of convergence, J. Acoust. Soc. Am. 97 (1995) 62-71.

[25] C. Prada, F. Wu, and M. Fink, The iterative time reversal mirror: A solution to self-focusing in the pulse echo mode, J. Acoust. Soc. Am. 90 (1991) 1119-1129.